

The homogeneous internal structure of CM-like asteroid (41) Daphne^{★, ★★}

B. Carry¹, F. Vachier², J. Berthier², M. Marsset³, P. Vernazza⁴, J. Grice^{1,5}, W. J. Merline⁶, E. Lagadec¹, A. Fienga⁷, A. Conrad⁸, E. Podlewska-Gaca^{9,11}, T. Santana-Ros⁹, M. Viikinkoski¹², J. Hanuš¹⁴, C. Dumas¹⁵, J. D. Drummond¹⁶, P. M. Tamblyn^{6,17}, C. R. Chapman⁶, R. Behrend¹⁸, L. Bernasconi¹⁸, P. Bartczak⁹, Z. Benkhaldoun¹⁰, M. Birlan², J. Castillo-Rogez¹⁹, F. Cipriani²⁰, F. Colas², A. Drouard⁴, J. Ďurech¹⁴, B. L. Enke⁶, S. Fauvaud^{18,21}, M. Ferrais²², R. Fetick⁴, T. Fusco⁴, M. Gillon²², E. Jehin²², L. Jordá⁴, M. Kaasalainen¹², M. Keppler¹³, A. Kryszczynska⁹, P. Lamy⁴, F. Marchis²³, A. Marciniak⁹, T. Michalowski⁹, P. Michel¹, M. Pajuelo^{2,24}, P. Tanga¹, A. Vigan⁴, B. Warner²⁵, O. Witasse²⁰, B. Yang²⁶, and A. Zurlo^{4,27,28}

(Affiliations can be found after the references)

Received 2018; accepted 2019-01-07

ABSTRACT

Context. CM-like asteroids (Ch and Cgh classes) are a major population within the broader C-complex, encompassing about 10% of the mass of the main asteroid belt. Their internal structure has been predicted to be homogeneous, based on their compositional similarity as inferred from spectroscopy (Vernazza et al., 2016, AJ 152, 154) and numerical modeling of their early thermal evolution (Bland & Travis, 2017, Sci. Adv. 3, e1602514).

Aims. Here we aim to test this hypothesis by deriving the density of the CM-like asteroid (41) Daphne from detailed modeling of its shape and the orbit of its small satellite.

Methods. We observed Daphne and its satellite within our imaging survey with the Very Large Telescope extreme adaptive-optics SPHERE/ZIMPOL camera (ID 199.C-0074, PI P. Vernazza) and complemented this data set with earlier Keck/NIRC2 and VLT/NACO observations. We analyzed the dynamics of the satellite with our Genoid meta-heuristic algorithm. Combining our high-angular resolution images with optical lightcurves and stellar occultations, we determine the spin period, orientation, and 3-D shape, using our ADAM shape modeling algorithm.

Results. The satellite orbits Daphne on an equatorial, quasi-circular, prograde orbit, like the satellites of many other large main-belt asteroids. The shape model of Daphne reveals several large flat areas that could be large impact craters. The mass determined from this orbit combined with the volume computed from the shape model implies a density for Daphne of $1.77 \pm 0.26 \text{ g}\cdot\text{cm}^{-3}$ (3σ). This density is consistent with a primordial CM-like homogeneous internal structure with some level of macroporosity ($\approx 17\%$).

Conclusions. Based on our analysis of the density of Daphne and 75 other Ch/Cgh-type asteroids gathered from the literature, we conclude that the primordial internal structure of the CM parent bodies was homogeneous.

Key words. Minor planets, asteroids: general – Minor planets, asteroids: individual: (41) Daphne – Methods: observational – Techniques: high angular resolution

1. Introduction

The C-complex encompasses 50% of the mass of the asteroid belt (or 14% if the four largest bodies, Ceres, Vesta, Pallas and Hygeia, are disregarded, DeMeo & Carry, 2013, 2014). Within this complex, the Ch- and Cgh-types are defined by the presence of an absorption band around $0.7 \mu\text{m}$, and a UV-dropoff (sharper for the Cgh). These have been estimated to represent between 30% and 65% by number (Rivkin, 2012; Fornasier et al., 2014), and are associated with CM chondrites (namely the Ch- and Cgh-types, see Vilas et al., 1993; Burbine, 1998; Bus & Binzel, 2002; DeMeo et al., 2009; Lantz et al., 2013; Fornasier et al.,

2014; Vernazza et al., 2016; Takir et al., 2013). In other words, CM-like bodies represent a significant fraction of the C-complex population and encompass about 10% of the mass of all main-belt asteroids. They are spread over the entire Main Belt, and are found at all diameters (e.g., Rivkin, 2012; Fornasier et al., 2014).

Their absorption band at $0.7 \mu\text{m}$ has been associated with phyllosilicates (Villas & Sykes, 1996). This is supported by the presence of a phyllosilicate band near $2.8 \mu\text{m}$ (commonly called the $3 \mu\text{m}$ absorption, Rivkin et al., 2015), as well as a shallow band at $2.33 \mu\text{m}$. The $2.8 \mu\text{m}$ band is very similar to that seen in the B-type asteroid (2) Pallas (Takir & Emery, 2012; Rivkin et al., 2015) and interpreted as being due to serpentine (e.g., Takir et al., 2013). The $2.33 \mu\text{m}$ band is also associated with the serpentine group (i.e., hydrous magnesium-iron phyllosilicates, Beck et al., 2018).

The meteorites originating from these bodies, the CM chondrites, represent 1.6% of all falls (Scott, 2007). Together with CI carbonaceous chondrites, they represent the most chemically primitive meteorites (i.e., closest to the solar composition, Scott, 2007) while paradoxically having suffered extensive hydration (e.g., Alexander et al., 2013). This aqueous alteration took place

* Based on observations made with 1) ESO Telescopes at the La Silla Paranal Observatory under programs 281.C-5011 (PI Dumas), 099.D-0098 (SPHERE GTO), and 199.C-0074(A) (PI Vernazza); and 2) the W. M. Keck Observatory, which is operated as a scientific partnership among the California Institute of Technology, the University of California and the National Aeronautics and Space Administration. The Observatory was made possible by the generous financial support of the W. M. Keck Foundation.

** The reduced and deconvolved AO images and the 3-D shape model are publicly available at <http://observations.lam.fr/astero/>

at low temperature, and thermal alteration of CM parent bodies peaked around 120°C (e.g., Dufresne & Anders, 1962; Zolensky et al., 1989, 1997; Guo & Eiler, 2007), and went up to 150°C as revealed by the formation of dolomite carbonates (Lee et al., 2014). As such, they are thought to have formed from a mixture of ice and dust where water ice was subsequently brought to a liquid state via the radioactive decay of ^{26}Al contained in dust particles, leading to the aqueous alteration of a significant fraction of the dust (see, e.g., Krot et al., 2006).

Recently, Vernazza et al. (2016) made a spectral survey of 70 Ch/Cgh asteroids, which included large 200+ km deemed-primordial bodies, but also objects as small as 15 km diameter, presumed to be the collisional fragments of dynamical families created from large bodies. This allowed a probe of the internal composition of prior, larger parent bodies. These authors interpreted the spectral diversity, already reported elsewhere (e.g., Vilas, 1994; Fornasier et al., 1999, 2014), as resulting mainly from a variation of the average regolith grain size rather than to different thermal histories (Fornasier et al., 2014; Rivkin et al., 2015), although differences in band depths and centers also argue for some heterogeneity in mineral abundances (Burbine, 1998; Cloutis et al., 2011; Fornasier et al., 2014). This evidence points toward an overall homogeneous internal structure for the parent bodies of CM chondrites.

The thermal modeling of the early internal structure of CM parent bodies by Bland & Travis (2017) supports this conclusion. They showed that convection may have prevented strong thermal gradients and differentiation of material. Starting from the accretion of dust and ices beyond the snow line (Scott et al., 2018), the original non-lithified structure of CM parent bodies has allowed large-scale circulation of material. This model explains both the limited temperature experienced by CM parent bodies, and the small-scale heterogeneity (such as temperature and redox state observed at the hundred of micrometer level, see Fujiya et al., 2015) observed in CM chondrites (Guo & Eiler, 2007; Bland & Travis, 2017).

To test this model, we sought to gather evidence for or against an originally differentiated internal structure within large Ch/Cgh asteroids. Our goal was to measure their bulk density, which, when compared with the density of CM chondrites, can reveal the presence, or absence, of denser material in their interior. Determination of a density requires both a mass and a volume. Masses for larger objects can be determined by their gravitational effects on other bodies, but the precision is often low, and is particularly problematic for objects of low mass (see Carry, 2012, for a discussion on the precision and biases in mass determination). If any object is binary, however, the orbit of the satellite yields the primary mass directly. Therefore, binary asteroids are crucial to establish solid and accurate references on which a larger population can be analyzed.

The present article focuses on asteroid (41) Daphne as representative of the Ch spectral class, around which a satellite was discovered in 2008 (S/2008 (41) 1, which we call *Peneius*¹, Conrad et al., 2008). Daphne was observed within a survey we are currently conducting (ID 199.C-0074, PI P. Vernazza) to image a substantial fraction of main-belt asteroids larger than 100 km in diameter, sampling the main compositional classes (see Vernazza et al., 2018, for a description of the survey). We image these asteroids throughout their rotation at high angular-resolution with the SPHERE/ZIMPOL extreme adaptive-optics (AO) camera (Beuzit et al., 2008; Thalmann et al., 2008) mounted on the European Southern Observatory (ESO) Very Large Telescope (VLT). The high-quality correction delivered by the AO system of SPHERE (Fusco et al., 2006, 2014) compared to previous generations of AO cameras, and the use of shorter wavelength (visible R band compared to the near-infrared J/H/K bands typically used with previous cameras), provides a twofold to threefold improvement in angular resolution. This sharper resolution allows the detailed modeling of asteroid shapes and enhanced satellite detection capability, as recently illustrated on the main-belt asteroids (3) Juno, (6) Hebe, (16) Psyche, (89) Julia, (107) Camilla, and (130) Elektra (Viikinkoski et al., 2015, 2018; Marsset et al., 2016, 2017a,b; Yang et al., 2016; Hanuš et al., 2017a; Pajuelo et al., 2018; Vernazza et al., 2018).

The article is organized as follows: we first describe our observations in Section 2, followed by the determination of the 3-D shape model (Section 2.2), the mutual orbit of Daphne and its satellite (Section 2.3), and the diameter and spectrum of the satellite itself (Section 2.4). Based on the density of (41) Daphne and a compilation of mass and diameter estimates from the literature, we then discuss the internal structure of CM parent bodies in Section 3.

2. Observations

Daphne was imaged with ZIMPOL once in May 2017 and three times in August 2018. We also compile 24 epochs of high-angular resolution and high-contrast images (Table B.1) from large ground-based telescopes equipped with adaptive-optics (AO) cameras: NIRC2 at Keck (van Dam et al., 2004) and NACO at ESO VLT (Rousset et al., 2003).

We process the ZIMPOL data with the ESO pipeline (see details in Vernazza et al., 2018). We then reduce all other imaging epochs with the same suite of IDL routines for consistency. The basic data reduction encompasses bad pixel mapping and removal by median interpolation, sky subtraction, and flat-field correction, following the steps described in Carry et al. (2008). We then use *Mistral*, a myopic deconvolution algorithm optimized for celestial targets with sharp boundaries (Fusco et al., 2002; Mugnier et al., 2004), to deconvolve the images and enhance their angular resolution for shape modeling purposes. The results of this approach have already been demonstrated elsewhere (e.g., Witasse et al., 2006; Drummond et al., 2014). In parallel, the diffused halo of light surrounding Daphne was removed by subtracting concentric annuli (as described thoroughly in Pajuelo et al., 2018) for satellite detection.

We complement this data set with an additional epoch of Daphne in May 2017 with the SPHERE integral-field spectrograph (IFS, Claudi et al., 2008) to acquire the near-infrared spectrum of its satellite *Peneius*. This epoch was obtained within the “Other Science” program (ID: 099.D-0098, PI J.-L. Beuzit) of the guaranteed-time observations (GTO) of the SPHERE consortium. The aim of this program is to illustrate SPHERE’s capabilities in science topics other than its primary goal: direct imaging of planets and disks. The IFS data were reduced using the SPHERE consortium pipeline, which includes bad pixel removal, sky subtraction, flat-field correction, and wavelength calibration.

Together with these images, we retrieve nine stellar occultations by Daphne compiled on the PDS by Dunham et al. (2017). We convert the locations of observers and disappearance timings into chords on the plane of the sky using the recipes by Berthier (1999). We detail the circumstances of observation of these occultations in Table B.2.

¹ pronounced “peh-NEH-oss”

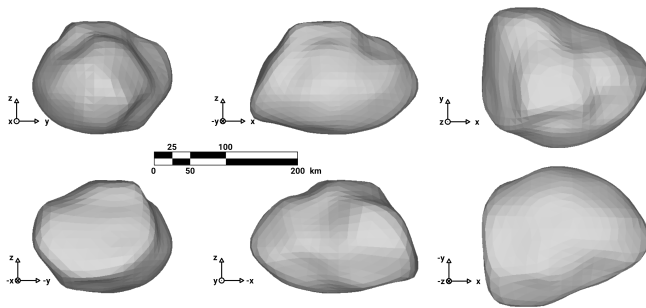


Fig. 1: Views of the shape model of Daphne. The X, Y, and Z axes are aligned along the principal axes of inertia.

We also compile 29 optical lightcurves, from the historical works of Scaltriti & Zappala (1977), Barucci (1983), Barucci et al. (1985), and Weidenschilling et al. (1987, 1990), used by Kaasalainen et al. (2002) and Hanuš et al. (2017b) to reconstruct the 3-D shape of Daphne. We complement this data set with twelve lightcurves obtained by amateur astronomers, two lightcurves obtained with the 60 cm André Peyrot telescope mounted at Les Makes observatory on Réunion Island (operated as a partnership among Les Makes Observatory and the IMCCE, Paris Observatory), one lightcurve obtained with the Antarctic Search for Transiting ExoPlanet (ASTEP) telescope (Daban et al., 2010) during its commissioning at the Observatoire de la Côte d'Azur in Nice (Matter et al., 2011), and extract three serendipitously observed lightcurves from the Super-WASP image archive (Grice et al., 2017). The details of these lightcurves are provided in Table B.3.

2.1. Properties of Daphne and its satellite

2.2. Spin and 3-D shape

We determine the spin properties (rotation period and spin-vector coordinates) and reconstruct the 3-D shape of Daphne with the open-source² ADAM algorithm (Viikinkoski et al., 2015). ADAM uses the Levenberg-Marquardt optimization algorithm to find the spin and 3-D shape that best reproduce the lightcurves, stellar occultation chords, and disk-resolved images simultaneously by comparing the observations with synthetic data generated by the model at each step.

The best-fit solution displayed in Fig. 1, the details of which are listed in Table 1, has a sidereal rotation period P_s of 5.98798 h and spin-vector ecliptic coordinates of $(199^\circ, -33^\circ)$, very similar to the results from convex shape modeling from lightcurves only by Kaasalainen et al. (2002) and multi-data shape reconstruction from a slightly different data set with ADAM by Hanuš et al. (2017b). The shape model is of an irregular body with several large flat areas, putative impact basins, and has a spherical-volume-equivalent diameter \mathcal{D} of 187 ± 21.5 km (3σ uncertainty). We present all the data compared with the predictions from the shape model in Appendix B.

An almost similar shape model and spin solution had been previously reported by Carry (2009) with the multi-data KOALA shape reconstruction algorithm (based on the same algorithm as ADAM but with different implementation, Carry et al., 2010a; Kaasalainen, 2011). Because KOALA has been validated by comparing the shape model of (21) Lutetia (Carry et al., 2010b; Drummond et al., 2010) with the images returned by

Table 1: Spin solution (coordinates in ecliptic and equatorial J2000 reference frames) and shape model parameters (the overall shape is reported as the $a > b > c$ diameters of a triaxial ellipsoid fit to the shape model). All uncertainties are reported at 3σ .

Parameter	Symbol	Value	Unc.	Unit
Sidereal period	P_s	5.987981	6.10^{-5}	hour
Longitude	λ	199.4	5.	deg.
Latitude	β	-31.9	5.	deg.
Right ascension	α	183.5	5.	deg.
Declination	δ	-36.6	5.	deg.
Ref. epoch	T_0	2444771.750		
Diameter	\mathcal{D}	187	21.5	km
Volume	V	$3.39 \cdot 10^6$	$7.1 \cdot 10^5$	km^3
Diam. a	a	237.9	21.5	km
Diam. b	b	184.8	21.5	km
Diam. c	c	156.0	21.5	km
Axes ratio	a/b	1.29	0.19	
Axes ratio	b/c	1.18	0.21	
Axes ratio	a/c	1.52	0.25	

the ESA Rosetta mission during its flyby of the asteroid (Sierks et al., 2011; Carry et al., 2012), the agreement between the two models provides solid evidence for the reliability of both ADAM and of the shape model of Daphne.

While there is a significant spread of diameter estimates in the literature (average diameter of 192 ± 38 km), all the estimates based on direct measurements, i.e. stellar occultations, disk-resolved imaging, mid-infrared interferometry, are narrowly clustered around our value: 188 ± 14 km (3σ deviation, see Table A.1). In particular, the mid-infrared interferometric observations by Matter et al. (2011) provide an independent confirmation, being based on a totally different data set. These authors analyzed their interferometric visibilities using the convex shape model of Kaasalainen et al. (2002) and the non-convex shape model of Carry (2009), almost identical to the model presented here. The associated diameters differ by 15 km, showing how the determination of diameter is sensitive to the shape of the object. Their best-fit diameter associated with the non-convex model was 185.5 ± 10.5 km (3σ), supporting the present value.

We define the prime meridian of Daphne to be along its longest axis, on which a hill, which we call the nose, is present at the equator (elevation of 11 km above the reference ellipsoid, see the map in Fig. 2). Several flat regions (hereafter A, B, C) can be identified in the images and on the shape model, as well as a clear depression (D). The three flat areas are located near both poles, and on the opposite side of the nose. These flat areas and the depression are large compared with the diameter of Daphne and may be indicative of large impact basins not modeled because concavities could not be detected with the available data (Ďurech & Kaasalainen, 2003; Devogèle et al., 2015). The central location and overall dimensions of these features, including the ratio of their surface-equivalent diameter to the diameter of Daphne, are listed in Table 2.

2.3. Dynamics of the system

On each image, we measure the relative position of the satellite with respect to center of light of the primary by adjusting a 2-D gaussian on the primary using the unmodified images and another on the satellite using the halo-removed images (Fig. 3). We

² <https://github.com/matvii/adam>

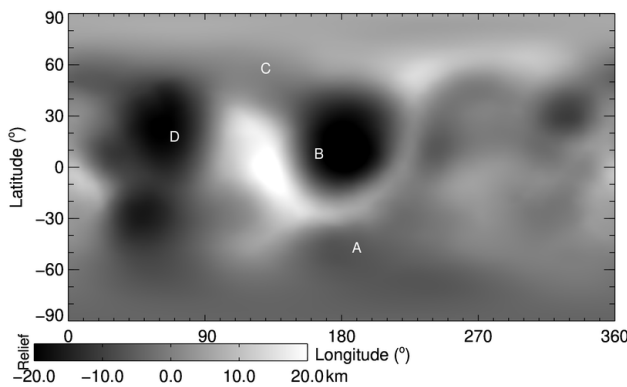


Fig. 2: Topography of Daphne, measured in kilometers with respect to its reference ellipsoid (Table 1). The putative depression is marked by the letter D, while the three flat areas are labeled A, B, and C. They may appear as circular depressions here (in particular B) because the topography is measured with respect to an ellipsoid.

Table 2: Dimensions (semi-axes \mathcal{L}_a and \mathcal{L}_b , surface area \mathcal{A} , and fraction f of Daphne's diameter) and planetocentric coordinates (λ_c, β_c) of the four notable topographic features of Daphne.

	A	B	C	D	Unit
λ_c	190 ± 5	165 ± 5	130 ± 5	60 ± 5	deg.
β_c	-50 ± 5	$+5 \pm 5$	$+55 \pm 5$	$+19 \pm 5$	deg.
\mathcal{L}_a	60 ± 5	68 ± 5	45 ± 5	42 ± 3	km
\mathcal{L}_b	48 ± 5	42 ± 5	45 ± 5	42 ± 3	km
\mathcal{A}	8.7 ± 3.3	9.0 ± 3.3	6.3 ± 2.8	5.5 ± 0.8	10^3 km^2
f	56 ± 10	57 ± 10	47 ± 10	44 ± 3	%

use the meta-heuristic algorithm Genoid (Vachier et al., 2012) to find the set of orbital parameters that best fit the observations. The orbital parameter space is usually 6-D for a simple Keplerian motion: orbital period, eccentricity, inclination, longitude of the ascending node, argument of periaapsis, and time of passage to the periaapsis. More dimensions are required if the gravitational potential is not central, such as in accounting for a gravitational quadrupole J_2 . Genoid explores this parameter space in successive generations of orbital solutions, randomly merging the parameters of the best solutions to create newer generations. In combination with this broad exploration of the parameter space, Genoid uses gradient descent at each generation to find the minimum closest to each best-trial solution.

The reliability of this approach has been assessed during a stellar occultation by (87) Sylvia in 2013. We had used Genoid to predict the position of its largest satellite Romulus before the event, placing observers on the occultation path of the satellite. Four different observers detected an occultation by Romulus at only 13.5 km off the predicted position (Berthier et al., 2014).

The best-fit orbit adjusts the 30 positions with a root-mean square (RMS) residual of 8.3 mas only, i.e., smaller than the pixel size of most observations (21 out of 30 taken with NACO/VLT and NIRC2/Keck, see Table C.1). The observations, covering 3783 days or 3326 revolutions, provide solid constraints on the orbital period ($1.137\,446 \pm 0.000\,009$ day). The satellite orbits Daphne on a Keplerian, equatorial, and prograde orbit, slightly eccentric (Table 3), at a distance of only 7.4 primary radii. We searched for a signature of the gravitational

Table 3: Orbital elements of *Peneius*, the satellite of Daphne, expressed in EQJ2000, obtained with Genoid: orbital period P , semi-major axis a , eccentricity e , inclination i , longitude of the ascending node Ω , argument of pericenter ω , time of pericenter t_p . The number of observations and RMS between predicted and observed positions are also provided. Finally, we report the derived primary mass M , the ecliptic J2000 coordinates of the orbital pole (λ_p, β_p), the equatorial J2000 coordinates of the orbital pole (α_p, δ_p), and the orbital inclination (Λ) with respect to the equator of Daphne. Uncertainties are given at 3σ .

Observing data set		
Number of observations	30	
Time span (days)	3783	
RMS (mas)	8.3	
Orbital elements EQJ2000		
P (day)	1.137 446	$\pm 0.000\,009$
a (km)	463.5	± 22.8
e	0.009	± 0.021
i ($^\circ$)	128.1	± 6.2
Ω ($^\circ$)	272.7	± 5.7
ω ($^\circ$)	171.9	± 37.6
t_p (JD)	2454550.586985	± 0.117331
Derived parameters		
M ($\times 10^{18}$ kg)	6.10	± 0.89
λ_p, β_p ($^\circ$)	197, -33	$\pm 6, 7$
α_p, δ_p ($^\circ$)	182, -38	$\pm 5, 7$
Λ ($^\circ$)	2	± 4

quadrupole J_2 but the poor time coverage of the astrometry with a gap of nine years between the positions in 2008 and the two in 2017 precluded any firm conclusion. A regular follow-up of the position of S/2008 (41) 1 is required to conclude on the J_2 of Daphne. These orbital characteristics argue in favor of a formation of the satellite by impact excavation, and re-accumulation of material in orbit, followed by tidal circularization (Weidenschilling et al., 1989; Merline et al., 2002; Durda et al., 2004; Margot et al., 2015).

2.4. Spectrum and diameter of the satellite

We recorded the near-infrared spectra of Daphne and its satellite with SPHERE/IFS. Telluric features were removed by observing the nearby star HD 102085 (G3V). Similarly to previous sections, the bright halo of Daphne that contaminated the spectrum of the moon was removed. This was achieved by measuring the background at the location of the moon for each pixel as the median value of the area defined as a 40×1 -pixel arc centered on Daphne. To estimate the uncertainty and potential bias on photometry (at each wavelength) introduced by this method, we performed a number of simulations (similarly to our study of the satellite of Camilla, see Pajuelo et al., 2018).

We added synthetic companions on the 39 spectral images of the spectro-imaging cube, at a similar separation to the satellite (≈ 300 mas) and random position angles from the primary. The simulated sources were modeled as the point-spread function from the calibration star images scaled in brightness. The halo from Daphne was then removed from these simulated images using the method described above, and the flux of the simulated companion measured by adjusting a 2D-Gaussian profile

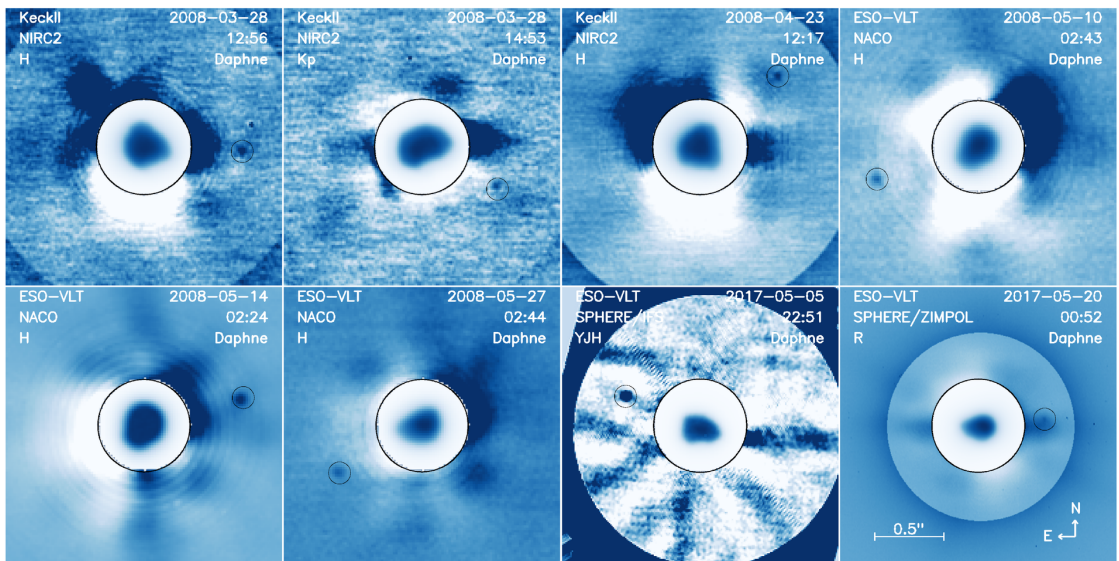


Fig. 3: Example images of Daphne and its satellite. Each panel represents a different epoch. The image is displayed in the inner circle, showing the irregular shape of Daphne. The outer region shows the images after halo removal, showing the satellite (highlighted by a small circle). On each panel the telescope, instrument, filter, and UTC date are reported.

(see Sect. 2.3). Based on a total statistics of 100 simulated companions, we find that the median loss of flux at each wavelength is $13 \pm 9\%$ and that the spectral slope is affected ($-0.50\% / 100\text{nm}$ on average).

The measured slope for each individual simulation, however, is not reliable, the standard deviation of all simulations being of $2.73\% / 100\text{nm}$. The value for each depends on the location (position angle) of the simulated satellite. Furthermore, the signal-to-noise ratio of the simulations range from virtually zero to four, with an average of 1.8 only. The spectrum of the satellite, therefore, is not reliable, being noisy and likely affected by strong slope effects.

From the integrated fluxes measured with the 2-D gaussian functions on Daphne and its satellite at each epoch (Fig. C.2 and Table C.1), we derived their magnitude difference to be 9.49 ± 0.32 . Combined with our determination of a diameter of $187 \pm 21.5\text{ km}$, we derive a diameter of $2.4^{+1.8}_{-1.1}\text{ km}$ for the satellite, under the assumption of a similar albedo for both. This assumption is supported by the multiple reports of spectral similarities between the components of multiple asteroid systems: (22) Kalliope (Laver et al., 2009), (90) Antiope (Polishook et al., 2009), (107) Camilla (Pajuelo et al., 2018), (130) Elektra (Yang et al., 2016), and (379) Huenna (DeMeo et al., 2011).

3. Implications on the internal structure

Using the volume determined from ADAM (Sect. 2.2) and the mass from Genoid (Sect. 2.3), we derive a bulk density of $1.77 \pm 0.26\text{ g}\cdot\text{cm}^{-3}$ (3σ uncertainty). This value is smaller but marginally consistent with the typical density of the CM carbonaceous chondrites, at $2.13 \pm 0.57\text{ g}\cdot\text{cm}^{-3}$ (3σ , Consolmagno et al., 2008). Comparing these two density values implies a macroporosity of $17 \pm 3\%$.

As visible in Fig. 4, Ch and Cgh asteroids over two orders of magnitude in mass follow the same trend and have a density smaller than that of CM meteorites, although there is definitively some scatter due to large uncertainties and biases in the determination of their density (see Appendix D for the complete list of estimates, and Carry, 2012, for a discussion on the reliabil-

ity of mass, diameter, and density estimates). The distribution of all density estimates weighted by their respective uncertainty is Gaussian with an average value of $1.40^{+1.92}_{-1.40}\text{ g}\cdot\text{cm}^{-3}$. This value changes to $1.58 \pm 0.97\text{ g}\cdot\text{cm}^{-3}$ (3σ) by considering only the estimates with less than 20% relative uncertainty (represented by the blue curves in Fig. 4). This highlights the importance of the study of binary systems that can be angularly resolved to accurately determine both the volume and the mass, hence the density.

There are three large (150+ km) binary Ch-type asteroids: (41) Daphne, (121) Hermione, and (130) Elektra. The density of Hermione was estimated to $1.4^{+1.5}_{-0.6}\text{ g}\cdot\text{cm}^{-3}$ by Descamps et al. (2009) and $1.26 \pm 0.90\text{ g}\cdot\text{cm}^{-3}$ by Viikinkoski et al. (2017). The density of Elektra was reported as $1.60 \pm 0.39\text{ g}\cdot\text{cm}^{-3}$ by Hanuš et al. (2017a), based on the mass estimate by Marchis et al. (2008a) while the mass recently derived by Yang et al. (2016) leads to $1.50 \pm 0.36\text{ g}\cdot\text{cm}^{-3}$. These values are somewhat smaller than the density of the three other large Ch-types: (13) Egeria at $1.99 \pm 0.69\text{ g}\cdot\text{cm}^{-3}$, (19) Fortuna at $1.96 \pm 0.28\text{ g}\cdot\text{cm}^{-3}$, and (48) Doris at $1.63 \pm 0.74\text{ g}\cdot\text{cm}^{-3}$ (see Appendix D). The density of these six targets is systematically smaller than CM meteorites.

Over the wide range of mass spanned by the Ch/Cgh asteroids studied here (Fig. 4), the density appears roughly constant although there is a larger spread toward smaller diameters. This larger spread is likely due to larger uncertainties on the density estimates (the gravitational signature of asteroids become harder to detect toward smaller sizes, see Carry, 2012). Indeed, the report by Carry (2012) of a correlation between density and mass (or diameter) due to an increasing macroporosity toward smaller diameters mainly happens for objects smaller than 100 km. This density of Ch/Cgh asteroids systematically lower than that of CM meteorites has two implications.

First, the density of the largest Ch/Cgh asteroids argues against the presence of material denser than CM-like material in their interior, i.e., differentiation. If denser material was present, their macroporosity would have to be large to maintain their bulk density, contrarily to what is observed for 100-200+ km bodies (Carry, 2012). Together with the observed compositional homogeneity of Ch/Cgh asteroids (Vernazza et al., 2016), it supports

the idea of an originally undifferentiated internal structure of CM parent bodies. Because collisional fragments sample the interior of their parent bodies, this spectral homogeneity only modulated by grain sizes together with the density smaller than the surface analog material can be interpreted as evidence for a homogeneous internal structure, without differentiation, of the CM parent bodies. The thermal modeling in “giant mud balls” (non-lithified structure) proposed by [Bland & Travis \(2017\)](#) then provides an explanation for the observed peak temperature of 120°C (e.g., [Guo & Eiler, 2007](#)).

Second, the density of Ch/Cgh asteroids being systematically smaller than CM chondrite indicates the presence of large voids, or less dense material, in their interior. Given the extensive hydration suffered by CM chondrites (e.g., [Alexander et al., 2013](#)) and the detection of water ice on/near the surface of asteroids well-within the snowline (e.g., [Campins et al., 2010](#); [Küppers et al., 2014](#)), one cannot reject the hypothesis of the presence of water ice in Ch/Cgh asteroids. However, considering that all these objects have experienced numerous collisions over the history of the solar system, some macroporosity, i.e. voids, can be expected.

4. Conclusion

We have acquired high-angular resolution images and spectro-images of the binary Ch-type asteroid (41) Daphne from large ground-based telescopes, including the new generation extreme adaptive-optics SPHERE camera mounted on the ESO VLT. We determined the orbit of its small satellite Peneus from 30 observations of its position around Daphne, with an RMS of 8.3 mas only. Combining our disk-resolved images with optical lightcurves and stellar occultations, we determined the 3-D shape of (41) Daphne.

The derived density of $1.77 \pm 0.26 \text{ g}\cdot\text{cm}^{-3}$ provides a solid reference to interpret the density of Ch/Cgh asteroids. The density is available for 76 of them and is found systematically smaller than that of the associated CM carbonaceous chondrites ($2.13 \pm 0.57 \text{ g}\cdot\text{cm}^{-3}$, 3σ), including for the largest asteroids. This provides robust evidence for a primordial homogeneous internal structure of these asteroids, in agreement with the observation of compositionnal homogeneity among Ch/Cgh asteroids of very different diameters by [Vernazza et al. \(2016\)](#) and the modeling of their early thermal history by [Bland & Travis \(2017\)](#).

Acknowledgements

Some of the work presented here is based on observations collected at the European Organisation for Astronomical Research in the Southern Hemisphere under ESO programs 281.C-5011 (PI Dumas), 099.D-0098, (SPHERE GTO), and 199.C-0074(A) (PI Vernazza).

Some of the data presented herein were obtained at the W.M. Keck Observatory, which is operated as a scientific partnership among the California Institute of Technology, the University of California and the National Aeronautics and Space Administration. The Observatory was made possible by the generous financial support of the W.M. Keck Foundation.

This research has made use of the Keck Observatory Archive (KOA), which is operated by the W. M. Keck Observatory and the NASA Exoplanet Science Institute (NExSci), under contract with the National Aeronautics and Space Administration.

We thank the AGORA association which administrates the 60 cm telescope at Les Males observatory, under a financial

agreement with Paris Observatory. Thanks to A. Peyrot, J.-P. Teng for local support, and A. Klotz for helping with the robotizing.

Some of these observations were acquired under grants from the National Science Foundation and NASA to Merline (PI). B. Carry, A. Drouard, J. Grice and P. Vernazza were supported by CNRS/INSU/PNP. J. Hanus and J. Durech were supported by the grant 18-09470S of the Czech Science Foundation. The research leading to these results has received funding from the European Union’s Horizon 2020 Research and Innovation Programme, under Grant Agreement no 687378.

This paper makes use of data from the DR1 of the WASP data ([Butters et al., 2010](#)) as provided by the WASP consortium, and the computing and storage facilities at the CERIT Scientific Cloud, reg. no. CZ.1.05/3.2.00/08.0144 which is operated by Masaryk University, Czech Republic.

TRAPPIST-South is funded by the Belgian Fund for Scientific Research (Fond National de la Recherche Scientifique, FNRS) under the grant FRFC 2.5.594.09.F, with the participation of the Swiss FNS. TRAPPIST-North is a project funded by the University of Liège, and performed in collaboration with Cadi Ayyad University of Marrakesh. E. Jehin and M. Guillot are Belgian FNRS Senior Research Associates.

The authors wish to recognize and acknowledge the very significant cultural role and reverence that the summit of Mauna Kea has always had within the indigenous Hawaiian community. We are most fortunate to have the opportunity to conduct observations from this mountain.

Thanks to all the amateurs worldwide who regularly observe asteroid lightcurves and stellar occultations. Some co-authors of this study are amateurs who observed Daphne, and provided crucial data.

The authors acknowledge the use of the Virtual Observatory tools Miriade³ ([Berthier et al., 2008](#)), TOPCAT⁴, and STILTS⁵ ([Taylor, 2005](#)). This research used the SSOIS⁶ facility of the Canadian Astronomy Data Centre operated by the National Research Council of Canada with the support of the Canadian Space Agency ([Gwyn et al., 2012](#)).

Part of the data utilized in this publication were obtained and made available by the MIT-UH-IRTF Joint Campaign for NEO Reconnaissance, using SpeX spectrograph ([Rayner et al., 2003](#)). The IRTF is operated by the University of Hawaii under Cooperative Agreement no. NCC 5-538 with the National Aeronautics and Space Administration, Office of Space Science, Planetary Astronomy Program. The MIT component of this work is supported by NASA grant 09-NEOO009-0001, and by the National Science Foundation under Grants Nos. 0506716 and 0907766.

We wish to acknowledge Professor Robert Groves, Director of Basic Languages (Classics) of the University of Arizona, for his assistance in selecting the name for Daphne’s satellite.

References

- Alexander, C. M. O. ., Howard, K. T., Bowden, R., & Fogel, M. L. 2013, *Geochim. Cosmochim. Acta*, 123, 244
- Baer, J. & Chesley, S. R. 2017, *AJ*, 154, 76
- Baer, J., Chesley, S. R., & Matson, R. D. 2011, *AJ*, 141, 143
- Baer, J., Milani, A., Chesley, S. R., & Matson, R. D. 2008, in *Bulletin of the American Astronomical Society*, Vol. 40, 493
- Barucci, M. A. 1983, *Astronomy and Astrophysics Supplement Series*, 54, 471

³ Miriade: <http://vo.imcce.fr/webservices/miriade/>

⁴ TOPCAT: <http://www.star.bris.ac.uk/~mbt/topcat/>

⁵ STILTS: <http://www.star.bris.ac.uk/~mbt/stilts/>

⁶ SSOIS: <http://www.cadc-ccda.hia-ihc.nrc-cnrc.gc.ca/en/ssois>

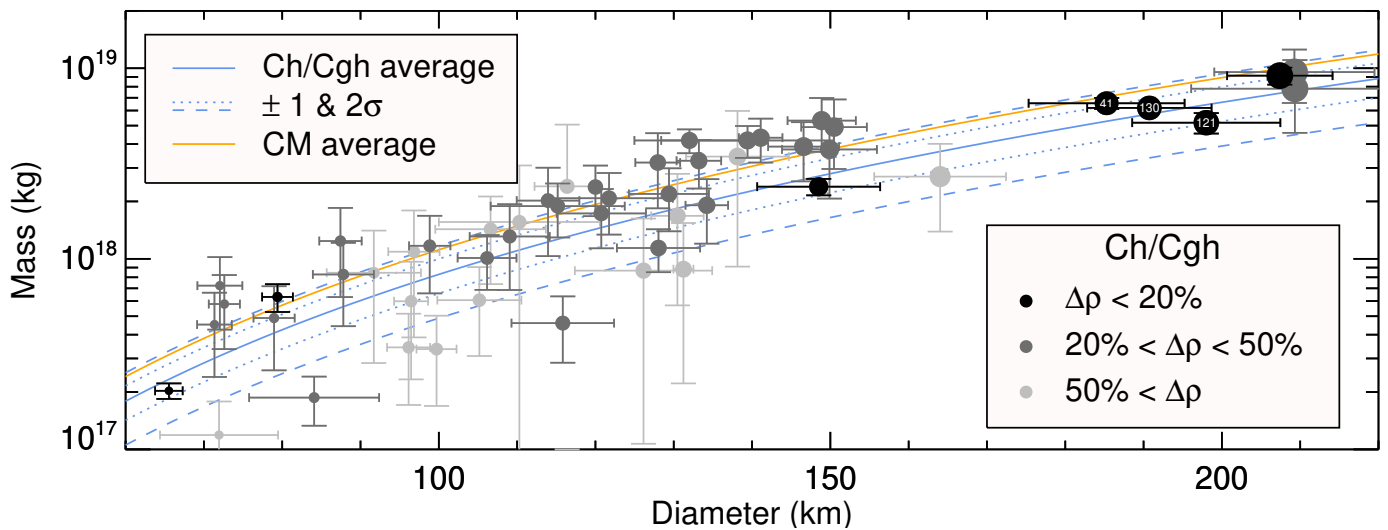


Fig. 4: Mass vs diameter distribution for 76 Ch/Cgh asteroids (grey circles). Those more precise than 50% and 20% are plotted as dark grey and black circles, respectively. Unreliable density estimates (below $0.5 \text{ g}\cdot\text{cm}^{-3}$) are not displayed. The three binary asteroids, (41) Daphne, (121) Hermione, (130) Elektra, are labeled. The solid and dashed blue curves represent the average density ($1.58 \text{ g}\cdot\text{cm}^{-3}$) and 1σ - 2σ ($\pm 0.33 \text{ g}\cdot\text{cm}^{-3}$) dispersion of the sample. The solid orange curve stands for the average density of CM chondrites at $2.13 \pm 0.57 \text{ g}\cdot\text{cm}^{-3}$ (3σ).

- Barucci, M. A., Fulchignoni, M., Burchi, R., & D'Ambrosio, V. 1985, Icarus, 61, 152
 Beck, P., Maturilli, A., Garenne, A., et al. 2018, Icarus, 313, 124
 Berthier, J. 1999, Notes scientifique et techniques du Bureau des longitudes, S064
 Berthier, J., Hestroffer, D., Carry, B., et al. 2008, LPI Contributions, 1405, 8374
 Berthier, J., Vachier, F., Marchis, F., Šurech, J., & Carry, B. 2014, Icarus, 239, 118
 Beuzit, J.-L., Feldt, M., Dohlen, K., et al. 2008, in SPIE, Vol. 7014, Ground-based and Airborne Instrumentation for Astronomy II, 701418
 Bland, P. A. & Travis, B. J. 2017, Science Advances, 3, e1602514
 Burbine, T. H. 1998, Meteoritics and Planetary Science, 33, 253
 Bus, S. J. & Binzel, R. P. 2002, Icarus, 158, 146
 Butters, O. W., West, R. G., Anderson, D. R., et al. 2010, A&A, 520, L10
 Campins, H., Hargrove, K., Pinilla-Alonso, N., et al. 2010, Nature, 464, 1320
 Carry, B. 2009, PhD thesis, Observatoire de Paris
 Carry, B. 2012, Planet. Space Sci., 73, 98
 Carry, B., Dumas, C., Fulchignoni, M., et al. 2008, A&A, 478, 235
 Carry, B., Dumas, C., Kaasalainen, M., et al. 2010a, Icarus, 205, 460
 Carry, B., Kaasalainen, M., Leyrat, C., et al. 2010b, A&A, 523, A94
 Carry, B., Kaasalainen, M., Merline, W. J., et al. 2012, Planet. Space Sci., 66, 200
 Claudi, R. U., Turatto, M., Gratton, R. G., et al. 2008, in SPIE, Vol. 7014, Ground-based and Airborne Instrumentation for Astronomy II, 70143E
 Cloutis, E. A., Hudon, P., Hiroi, T., Gaffey, M. J., & Mann, P. 2011, Icarus, 216, 309
 Conrad, A. R., Merline, W. J., Drummond, J. D., et al. 2008, IAU Circular, 8930, 2
 Consolmagno, G., Britt, D., & Macke, R. 2008, Chemie der Erde / Geochemistry, 68, 1
 Dabau, J.-B., Gouret, C., Guillot, T., et al. 2010, in Proc. SPIE, Vol. 7733, Society of Photo-Optical Instrumentation Engineers (SPIE) Conference Series
 DeMeo, F., Binzel, R. P., Slivan, S. M., & Bus, S. J. 2009, Icarus, 202, 160
 DeMeo, F. & Carry, B. 2013, Icarus, 226, 723
 DeMeo, F. & Carry, B. 2014, Nature, 505, 629
 DeMeo, F. E., Carry, B., Marchis, F., et al. 2011, Icarus, 212, 677
 Descamps, P., Marchis, F., Durech, J., et al. 2009, Icarus, 203, 88
 Devogèle, M., Rivet, J. P., Tanga, P., et al. 2015, MNRAS, 453, 2232
 Drummond, J. D., Carry, B., Merline, W. J., et al. 2014, Icarus, 236, 28
 Drummond, J. D., Conrad, A., Merline, W. J., et al. 2010, A&A, 523, A93
 Drummond, J. D., Merline, W. J., Conrad, A., et al. 2011, in AAS/Division for Planetary Sciences Meeting Abstracts, Vol. 43, AAS/Division for Planetary Sciences Meeting Abstracts #41, –
 Dufresne, E. R. & Anders, E. 1962, Geochim. Cosmochim. Acta, 26, 1085
 Dunham, D. W., Herald, D., Frappa, E., et al. 2017, Asteroid Occultations, NASA Planetary Data System, EAR-A-3-RDR-OCCULTATIONS-V15.0
 Durda, D. D., Bottke, W. F., Enke, B. L., et al. 2004, Icarus, 170, 243
 Šurech, J. & Kaasalainen, M. 2003, A&A, 404, 709
 Šurech, J., Kaasalainen, M., Herald, D., et al. 2011, Icarus, 214, 652
 Fienga, A. 2018, pers. comm.
 Fienga, A., Kuchynka, P., Laskar, J., Manche, H., & Gastineau, M. 2011, EPSC-DPS Joint Meeting 2011, 1879
 Fienga, A., Laskar, J., Morley, T., et al. 2009, A&A, 507, 1675
 Fienga, A., Manche, H., Laskar, J., Gastineau, M., & Verma, A. 2013, ArXiv e-prints
 Fienga, A., Manche, H., Laskar, J., Gastineau, M., & Verma, A. 2014, Scientific notes
 Folkner, W. M., Williams, J. G., & Boggs, D. H. 2009, IPN Progress Report, 42, 1
 Fornasier, S., Lantz, C., Barucci, M. A., & Lazzarin, M. 2014, Icarus, 233, 163
 Fornasier, S., Lazzarin, M., Barbieri, C., & Barucci, M. A. 1999, Astronomy and Astrophysics Supplement Series, 135, 65
 Fujiya, W., Sugiura, N., Marrocchi, Y., et al. 2015, Geochimica et Cosmochimica Acta, 161, 101
 Fusco, T., Conan, J.-M., Michau, V., & Rousset, G. 2002, in Proc. SPIE, Vol. 4538, Optics in Atmospheric Propagation and Adaptive Systems IV, ed. A. Kohnle, J. D. Ginglewski, & T. J. Schmugge, 144–155
 Fusco, T., Rousset, G., Sauvage, J.-F., et al. 2006, Optics Express, 14, 7515
 Fusco, T., Sauvage, J.-F., Petit, C., et al. 2014, in Proc. SPIE, Vol. 9148, Adaptive Optics Systems IV, 91481U
 Goffin, E. 2014, A&A, 565, A56
 Grav, T., Mainzer, A. K., Bauer, J., et al. 2012, ApJ, 744, 197
 Grice, J., Snodgrass, C., Green, S., Parley, N., & Carry, B. 2017, Asteroids, Comets, and Meteors: ACM 2017
 Guo, W. & Eiler, J. M. 2007, Geochim. Cosmochim. Acta, 71, 5565
 Gwyn, S. D. J., Hill, N., & Kavelaars, J. J. 2012, Publications of the Astronomical Society of the Pacific, 124, 579
 Hanuš, J., Šurech, J., Brož, M., et al. 2013a, A&A, 551, A67
 Hanuš, J., Marchis, F., & Šurech, J. 2013b, Icarus, 226, 1045
 Hanuš, J., Marchis, F., Viikinkoski, M., Yang, B., & Kaasalainen, M. 2017a, A&A, 599, A36
 Hanuš, J., Viikinkoski, M., Marchis, F., et al. 2017b, A&A, 601, A114
 Hasegawa, S., Müller, T. G., Kuroda, D., Takita, S., & Usui, F. 2013, Publications of the Astronomical Society of Japan, 65, 34
 Ivantsov, A. 2008, Planet. Space Sci., 56, 1857
 Kaasalainen, M. 2011, Inverse Problems and Imaging, 5, 37
 Kaasalainen, M., Torppa, J., & Piironen, J. 2002, A&A, 383, L19
 Kochetova, O. M. 2004, Solar System Research, 38, 66
 Kochetova, O. M. & Chernetko, Y. A. 2014, Solar System Research, 48, 295
 Konopliv, A. S., Asmar, S. W., Folkner, W. M., et al. 2011, Icarus, 211, 401
 Krásinsky, G. A., Pitjeva, E. V., Vasiliev, M. V., & Yagudina, E. I. 2001, in Communications of IAA of RAS
 Kretlow, M. 2014, Minor Planet Bulletin, 41, 194
 Krot, A. N., Hutcheon, I. D., Brearley, A. J., et al. 2006, Timescales and Settings for Alteration of Chondritic Meteorites, ed. D. S. Lauretta & H. Y. McSween, 525–553

- Kuchynka, P. & Folkner, W. M. 2013, Icarus, 222, 243
- Küppers, M., O'Rourke, L., Bockelée-Morvan, D., et al. 2014, Nature, 505, 525
- Lantz, C., Clark, B. E., Barucci, M. A., & Lauretta, D. S. 2013, A&A, 554, A138
- Laver, C., de Pater, I., Marchis, F., Ádámkovics, M., & Wong, M. H. 2009, Icarus, 204, 574
- Lee, M. R., Lindgren, P., & Soffe, M. R. 2014, Geochim. Cosmochim. Acta, 144, 126
- Marchis, F., Descamps, P., Baek, M., et al. 2008a, Icarus, 196, 97
- Marchis, F., Descamps, P., Berthier, J., et al. 2008b, Icarus, 195, 295
- Marchis, F., Enriquez, J. E., Emery, J. P., et al. 2012, Icarus, 221, 1130
- Marchis, F., Hestroffer, D., Descamps, P., et al. 2005, Icarus, 178, 450
- Marchis, F., Kaasalainen, M., Hom, E. F. Y., et al. 2006, Icarus, 185, 39
- Marciniak, A., Bartczak, P., Müller, T., et al. 2018, A&A, 610, A7
- Marciniak, A., Bartczak, P., Santana-Ros, T., et al. 2012, A&A, 545, A131
- Margot, J.-L., Pravec, P., Taylor, P., Carry, B., & Jacobson, S. 2015, Asteroid Systems: Binaries, Triples, and Pairs, ed. P. Michel, F. DeMeo, & W. F. Bottke (Univ. Arizona Press), 355–374
- Marsset, M., Carry, B., Dumas, C., et al. 2017a, A&A, 604, A64
- Marsset, M., Carry, B., Pajuelo, M., et al. 2017b, The Messenger, 169, 29
- Marsset, M., Carry, B., Yang, B., et al. 2016, IAU Circular, 9282
- Masiero, J. R., Mainzer, A. K., Grav, T., et al. 2011, ApJ, 741, 68
- Masiero, J. R., Mainzer, A. K., Grav, T., et al. 2012, ApJ, 759, L8
- Matter, A., Delbo, M., Ligori, S., Crouzet, N., & Tanga, P. 2011, Icarus, 215, 47
- Merline, W. J., Weidenschilling, S. J., Durda, D. D., et al. 2002, Asteroids III, 289
- Morrison, D. & Zellner, B. 2007, TRIAD Radiometric Diameters and Albedos, NASA Planetary Data System, EAR-A-COMPIL-5-TRIADRAD-V1.0
- Mugnier, L. M., Fusco, T., & Conan, J.-M. 2004, Journal of the Optical Society of America A, 21, 1841
- Nugent, C. R., Mainzer, A., Masiero, J., et al. 2015, ApJ, 814, 117
- Pajuelo, M., Carry, B., Vachier, F., et al. 2018, Icarus, 309, 134
- Pitjeva, E. V. 2013, Solar System Research, 47, 386
- Polishook, D., Brosch, N., Prialnik, D., & Kaspi, S. 2009, Meteoritics and Planetary Science, 44, 1955
- Rayner, J. T., Toomey, D. W., Onaka, P. M., et al. 2003, Publications of the Astronomical Society of the Pacific, 115, 362
- Rivkin, A. S. 2012, Icarus, 221, 744
- Rivkin, A. S., Thomas, C. A., Howell, E. S., & Emery, J. P. 2015, AJ, 150, 198
- Rousset, G., Lacombe, F., Puget, P., et al. 2003, SPIE, 4839, 140
- Ryan, E. L., Mizuno, D. R., Shenoy, S. S., et al. 2015, A&A, 578, A42
- Ryan, E. L. & Woodward, C. E. 2010, AJ, 140, 933
- Scaltriti, F. & Zappala, V. 1977, A&A, 56, 7
- Scott, E. R. D. 2007, Annual Review of Earth and Planetary Sciences, 35, 577
- Scott, E. R. D., Krot, A. N., & Sanders, I. S. 2018, ApJ, 854, 164
- Siers, H., Lamy, P., Barbieri, C., et al. 2011, Science, 334, 487
- Siltala, L. & Granvik, M. 2017, Icarus, 297, 149
- Somenzi, L., Fienga, A., Laskar, J., & Kuchynka, P. 2010, Planet. Space Sci., 58, 858
- Takir, D. & Emery, J. P. 2012, Icarus, 219, 641
- Takir, D., Emery, J. P., McSween, H. Y., et al. 2013, Meteoritics and Planetary Science, 48, 1618
- Taylor, M. B. 2005, in Astronomical Society of the Pacific Conference Series, Vol. 347, Astronomical Data Analysis Software and Systems XIV, ed. P. Shopbell, M. Britton, & R. Ebert, 29
- Tedesco, E. F., Egan, M. P., & Price, S. D. 2004a, MSX Infrared Minor Planet Survey, NASA Planetary Data System, MSX-A-SPIRIT3-5-SBN0003-MIMPS-V1.0
- Tedesco, E. F., Noah, P. V., Noah, M. C., & Price, S. D. 2004b, IRAS Minor Planet Survey, NASA Planetary Data System, IRAS-A-FPA-3-RDR-IMPS-V6.0
- Thalmann, C., Schmid, H. M., Boccaletti, A., et al. 2008, in Proc. SPIE, Vol. 7014, Ground-based and Airborne Instrumentation for Astronomy II, 70143F
- Usui, F., Kuroda, D., Müller, T. G., et al. 2011, Publications of the Astronomical Society of Japan, 63, 1117
- Vachier, F., Berthier, J., & Marchis, F. 2012, A&A, 543, A68
- van Dam, M. A., Le Mignant, D., & Macintosh, B. 2004, Applied Optics, 43, 5458
- Vernazza, P., Broz, M., Drouard, A., et al. 2018, A&A, A154
- Vernazza, P., Marsset, M., Beck, P., et al. 2016, AJ, 152, 54
- Viateau, B. 2000, A&A, 354, 725
- Viikinkoski, M., Hanuš, J., Kaasalainen, M., Marchis, F., & Durech, J. 2017, A&A, 607, A117
- Viikinkoski, M., Kaasalainen, M., & Durech, J. 2015, A&A, 576, A8
- Viikinkoski, M., Vernazza, P., Hanuš, J., et al. 2018, ArXiv e-prints, arXiv:1810.02771
- Vilas, F. 1994, Icarus, 111, 456
- Vilas, F., Larson, S. M., Hatch, E. C., & Jarvis, K. S. 1993, Icarus, 105, 67
- Vilas, F. & Sykes, M. V. 1996, Icarus, 124, 483
- Viswanathan, V., Fienga, A., Gastineau, M., & Laskar, J. 2017, Notes Scientifiques et Techniques de l'Institut de mécanique céleste, (ISSN 1621-3823), #108, ISBN 2-910015-79-3 , 2017, 39 pp., 108
- Weidenschilling, S. J., Chapman, C. R., Davis, D. R., Greenberg, R., & Levy, D. H. 1990, Icarus, 86, 402
- Weidenschilling, S. J., Chapman, C. R., Davis, D. R., et al. 1987, Icarus, 70, 191
- Weidenschilling, S. J., Paolicchi, P., & Zappala, V. 1989, Asteroids II, 643
- Witasse, O., Lebreton, J.-P., Bird, M. K., et al. 2006, Journal of Geophysical Research (Planets), 111, 7
- Yang, B., Wahhaj, Z., Beauvalet, L., et al. 2016, Astrophysical Journal Letter, 820, L35
- Zielenbach, W. 2011, AJ, 142, 120
- Zolensky, M. E., Bourcier, W. L., & Gooding, J. L. 1989, Icarus, 78, 411
- Zolensky, M. E., Mittlefehdlt, D. W., Lipschutz, M. E., et al. 1997, Geochim. Cosmochim. Acta, 61, 5099
-
- ¹ Université Côte d'Azur, Observatoire de la Côte d'Azur, CNRS, Laboratoire Lagrange, France e-mail: benoit.carry@oca.eu
- ² IMCCE, Observatoire de Paris, PSL Research University, CNRS, Sorbonne Universités, UPMC Univ Paris 06, Univ. Lille, France
- ³ Astrophysics Research Centre, Queen's University Belfast, BT7 1NN, UK
- ⁴ Aix Marseille Univ, CNRS, LAM, Laboratoire d'Astrophysique de Marseille, Marseille, France
- ⁵ Open University, School of Physical Sciences, The Open University, MK7 6AA, UK
- ⁶ Southwest Research Institute, Boulder, CO 80302, USA
- ⁷ Université Côte d'Azur, Observatoire de la Côte d'Azur, CNRS, Laboratoire GéoAzur, France
- ⁸ Large Binocular Telescope Observatory, University of Arizona, Tucson, AZ 85721, USA
- ⁹ Faculty of Physics, Astronomical Observatory Institute, Adam Mickiewicz University, ul. Śloneczna 36, 60-286 Poznań, Poland
- ¹⁰ Oukaimeden Observatory, High Energy Physics and Astrophysics Laboratory, Cadi Ayyad University, Marrakech, Morocco
- ¹¹ Institute of Physics, University of Szczecin, Wielkopolska 15, 70-453 Szczecin, Poland
- ¹² Department of Mathematics, Tampere University of Technology, PO Box 553, 33101, Tampere, Finland
- ¹³ Max Planck Institute for Astronomy, Königstuhl 17, D-69117, Heidelberg, Germany
- ¹⁴ Astronomical Institute, Faculty of Mathematics and Physics, Charles University, V Holešovičkách 2, 18000 Prague, Czech Republic
- ¹⁵ Thirty-Meter-Telescope, 100 West Walnut St, Suite 300, Pasadena, CA 91124, USA
- ¹⁶ Leidos, Starfire Optical Range, AFRL, Kirtland AFB, NM 87117, USA
- ¹⁷ Binary Astronomy, Aurora, CO 80012, USA
- ¹⁸ CdR & CdL Group: Lightcurves of Minor Planets and Variable Stars, Observatoire de Genève, CH-1290 Sauverny, Switzerland
- ¹⁹ Jet Propulsion Laboratory, California Institute of Technology, 4800 Oak Grove Drive, Pasadena, CA 91109, USA
- ²⁰ European Space Agency, ESTEC - Scientific Support Office, Keplerlaan 1, Noordwijk 2200 AG, The Netherlands
- ²¹ Observatoire du Bois de Bardon, 16110 Taponnat, France
- ²² Space sciences, Technologies and Astrophysics Research (STAR) Institute, Université de Liège, Allée du 6 Août 17, 4000 Liège, Belgium
- ²³ SETI Institute, Carl Sagan Center, 189 Bernardo Avenue, Mountain View CA 94043, USA
- ²⁴ Sección Física, Departamento de Ciencias, Pontificia Universidad Católica del Perú, Apartado 1761, Lima, Perú
- ²⁵ Center for Solar System Studies, 446 Sycamore Ave., Eaton, CO 80615, USA
- ²⁶ European Southern Observatory (ESO), Alonso de Cordova 3107, 1900 Casilla Vitacura, Santiago, Chile
- ²⁷ Núcleo de Astronomía, Facultad de Ingeniería y Ciencias, Universidad Diego Portales, Av. Ejercito 441, Santiago, Chile
- ²⁸ Escuela de Ingeniería Industrial, Facultad de Ingeniería y Ciencias, Universidad Diego Portales, Av. Ejercito 441, Santiago, Chile

Appendix A: Compilation of diameter and mass estimates

Table A.1: The diameter estimates (\mathcal{D}) of (41) Daphne collected in the literature. For each, the 3σ uncertainty, method, and bibliographic reference are reported. The methods are ADAM: Multidata 3-D Modeling, LCIMG: 3-D Model scaled with Imaging, LCOCC: 3-D Model scaled with Occultation, NEATM: Near-Earth Asteroid Thermal Model, STM: Standard Thermal Model, TPM: Thermophysical Model.

#	\mathcal{D} (km)	$\delta\mathcal{D}$ (km)	Method	Reference
1	203.00	60.90	STM	Morrison & Zellner (2007)
2	174.00	35.10	STM	Tedesco et al. (2004b)
3	172.43	12.24	STM	Ryan & Woodward (2010)
4	207.87	31.56	NEATM	Ryan & Woodward (2010)
5	187.00	60.00	LCOCC	Ďurech et al. (2011)
6	201.50	22.50	TPM	Matter et al. (2011)
7	185.50	10.50	TPM	Matter et al. (2011)
8	179.61	7.74	STM	Usui et al. (2011)
9	205.50	5.64	NEATM	Masiero et al. (2012)
10	186.00	81.00	LCIMG	Hanuš et al. (2013b)
11	198.74	185.13	NEATM	Nugent et al. (2015)
12	188.00	15.00	ADAM	Hanuš et al. (2017b)
13	187.00	21.50	ADAM	This work

Table A.2: The mass estimates (\mathcal{M}) of (41) Daphne collected in the literature. For each, the 3σ uncertainty, method, and bibliographic reference are reported. The methods are BGENO: Binary-Genoid, DEFL: Deflection, EPHEM: Ephemeris.

#	Mass (\mathcal{M}) ($\times 10^{18}$ kg)	Method	Reference
1	10.50 ± 2.99	EPHEM	Fienga et al. (2009)
2	7.90 ± 2.37	EPHEM	Folkner et al. (2009)
3	$8.43^{+10.56}_{-8.43}$	EPHEM	Konopliv et al. (2011)
4	$18.20^{+21.60}_{-18.20}$	DEFL	Zielenbach (2011)
5	$0.30^{+17.01}_{-0.30}$	DEFL	Zielenbach (2011)
6	$4.76^{+16.30}_{-4.76}$	DEFL	Zielenbach (2011)
7	$12.10^{+31.50}_{-12.10}$	DEFL	Zielenbach (2011)
8	10.20 ± 3.57	EPHEM	Fienga et al. (2011)
9	7.79 ± 5.40	EPHEM	Kuchynka & Folkner (2013)
10	8.29 ± 2.62	EPHEM	Pitjeva (2013)
11	7.13 ± 2.01	EPHEM	Fienga et al. (2014)
12	9.35 ± 4.17	DEFL	Goffin (2014)
13	$9.78^{+13.77}_{-9.78}$	DEFL	Kochetova & Chernetenko (2014)
14	4.44 ± 2.52	EPHEM	Fienga (2018)
15	6.10 ± 0.89	BGENO	This work

Appendix B: Shape modeling: data and model predictions

Table B.1: Date, telescope, camera, number of epochs (N_S), heliocentric distance (Δ), range to observer (r), phase angle (α), angular diameter (Θ), and program ID and Principal Investigator (PI) for each night of AO imaging observations.

	Date	Telescope	Instrument	N_S	Δ (au)	r (au)	α (°)	Θ (mas)	Prog. ID	PI
1	2002-12-29	Keck	NIRC2	1	2.65	1.91	16.4	135	C74N2	J.-L. Margot
2	2003-05-06	Keck	NIRC2	1	2.28	2.06	26.2	125	N17N2	W. J. Merline
3	2008-01-21	Keck	NIRC2	7	2.19	1.78	26.3	144	DDT	A. Conrad
4	2008-03-28	Keck	NIRC2	10	2.06	1.09	9.1	235	DDT	A. Conrad
5	2008-04-23	Keck	NIRC2	5	2.03	1.06	9.9	243	DDT	A. Conrad
6	2008-05-10	VLT	NACO	4	2.02	1.12	17.5	229	281.C-5011	C. Dumas
7	2008-05-14	VLT	NACO	2	2.02	1.14	19.1	225	281.C-5011	C. Dumas
8	2008-05-27	VLT	NACO	2	2.01	1.23	23.6	209	281.C-5011	C. Dumas
9	2010-11-30	Keck	NIRC2	1	3.50	2.60	7.6	99	U028N2	F. Marchis
10	2017-05-05	VLT	SPHERE/IFS	1	2.09	1.44	25.6	179	099.D-0098	J.-L. Beuzit
11	2017-05-20	VLT	SPHERE/ZIMPOL	1	2.06	1.56	28.3	164	199.C-0074	P. Vernazza
12	2018-08-05	VLT	SPHERE/ZIMPOL	3	2.80	1.90	11.7	136	199.C-0074	P. Vernazza

Table B.2: Date, number of positive and negative chords ($\#_p$ and $\#_n$), and average uncertainty in seconds (σ_s) and kilometers (σ_{km}) for each stellar occultation.

	Date	UT (h)	$\#_p$	$\#_n$	σ_s (s)	σ_{km} (km)
1	1999-07-02	20:27	21	3	1.21	46.150
2	2008-04-01	18:12	2	1	0.50	4.814
3	2012-01-09	10:39	1	3	1.00	3.224
4	2012-02-23	20:45	3	1	0.10	1.492
5	2012-03-02	18:49	1	4	2.00	3.411
6	2013-03-30	18:29	2	0	0.01	0.340
7	2013-09-05	22:26	4	2	0.44	7.655
8	2013-11-29	19:16	2	0	0.26	16.458
9	2016-01-17	22:42	19	0	0.41	1104.226

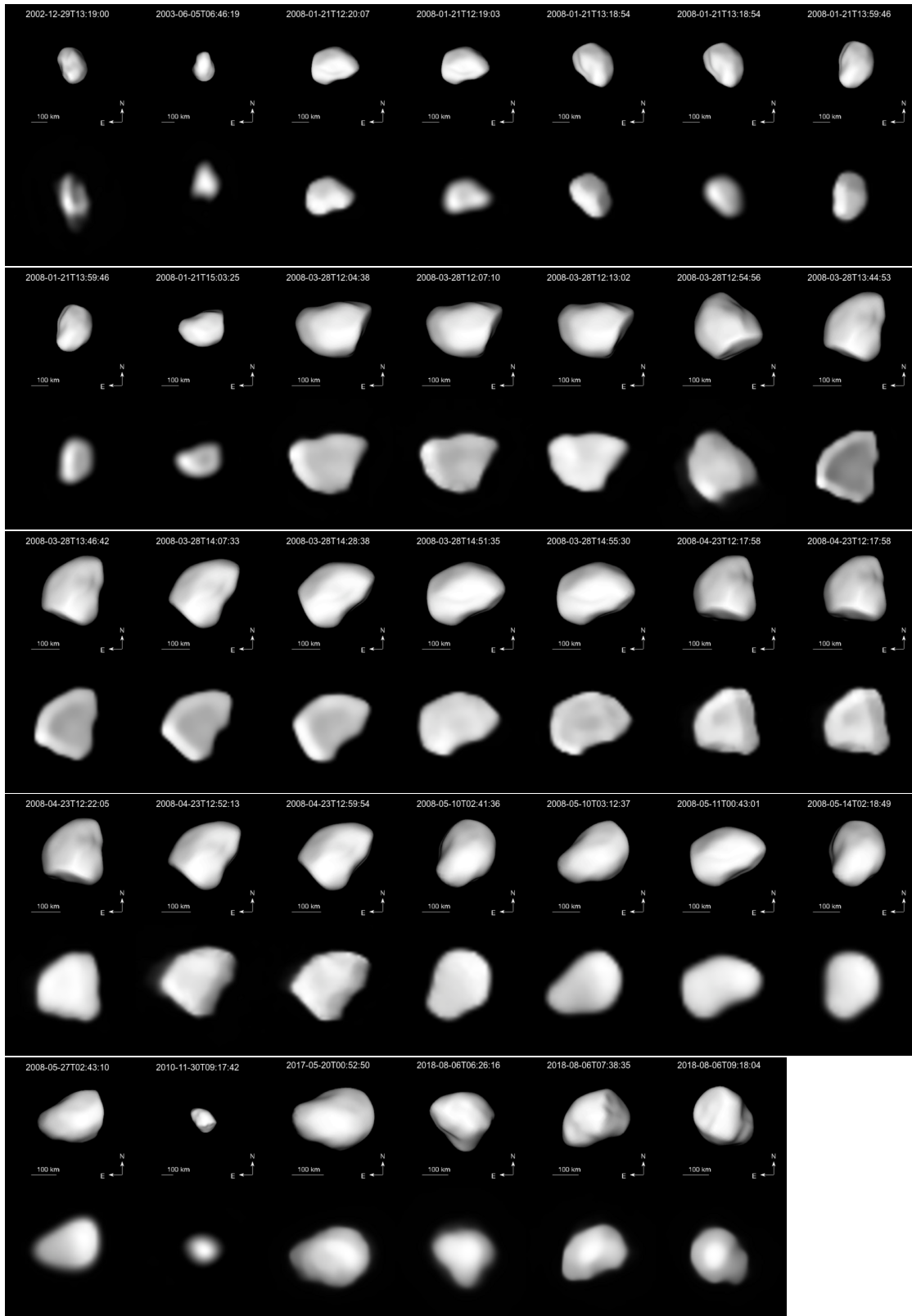


Fig. B.1: Comparison of the shape model (top image of each row), oriented and projected on the plane of the sky at the epoch of each disk-resolved observation (bottom image of each row). The brighter ring presents in some images (e.g., second row, last column) is an artifact from deconvolution.

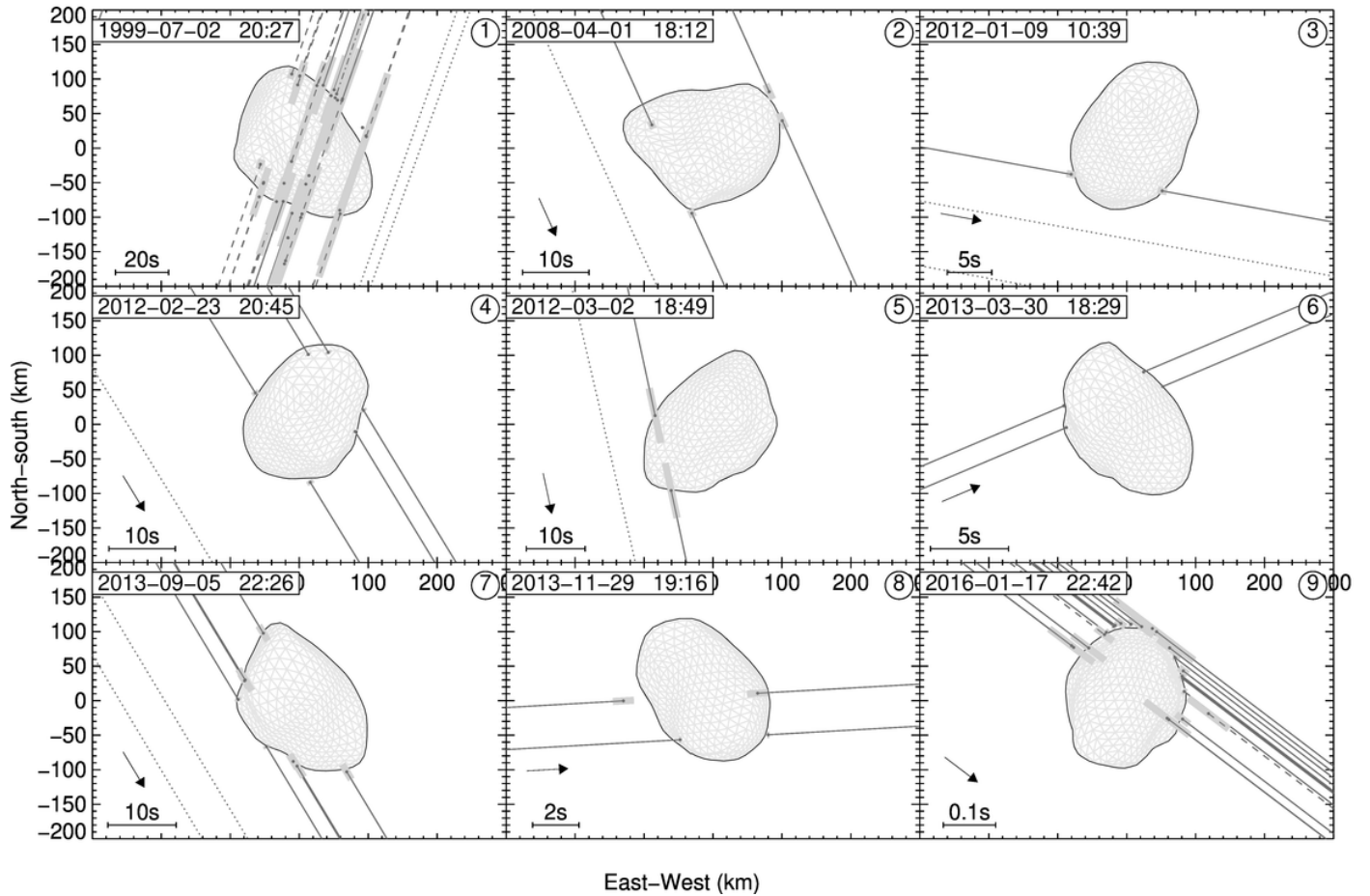


Fig. B.2: The eight stellar occultations by Daphne, compared with the shape model (profile in black and facets in light gray) projected on the plane of the sky at the time of the occultation. Negative chords are represented by dotted lines, visual timings by dashed lines, and electronic timings by solid lines. Disappearance and reappearances timings are marked by filled circles, and their uncertainty by gray rectangles.

Table B.3: Date, duration (\mathcal{L} , in hours), number of points (N_p), phase angle (α), filter, residual (against the shape model), and observers, for each lightcurve.

	Date	\mathcal{L} (h)	N_p	α ($^{\circ}$)	Filter	RMS (mag)	Observers
1	1976-04-26	6.2	188	18.4	V	0.024	Scaltriti & Zappala (1977)
2	1976-05-02	6.1	163	16.8	V	0.028	Scaltriti & Zappala (1977)
3	1976-05-31	3.8	130	13.8	V	0.029	Scaltriti & Zappala (1977)
4	1981-06-16	3.7	14	21.1	V	0.018	Weidenschilling et al. (1987)
5	1981-06-17	1.6	7	20.9	V	0.018	Weidenschilling et al. (1987)
6	1981-07-25	4.2	34	9.8	V	0.029	Barucci (1983)
7	1981-07-23	4.3	58	9.8	V	0.031	Barucci (1983)
8	1981-08-03	4.8	78	7.4	V	0.022	Barucci (1983)
9	1981-08-04	6.0	64	7.4	V	0.033	Barucci (1983)
10	1981-08-06	5.6	23	7.2	V	0.030	Weidenschilling et al. (1987)
11	1981-11-05	3.6	20	20.6	V	0.050	Weidenschilling et al. (1987)
12	1981-12-01	1.3	7	18.8	V	0.054	Weidenschilling et al. (1987)
13	1981-12-02	5.9	12	18.7	V	0.028	Weidenschilling et al. (1987)
14	1982-09-29	4.8	20	7.5	V	0.017	Weidenschilling et al. (1987)
15	1982-10-26	4.8	35	3.7	V	0.033	Barucci (1983)
16	1983-10-11	1.0	5	16.7	V	0.035	Weidenschilling et al. (1987)
17	1983-10-15	1.8	7	16.4	V	0.017	Weidenschilling et al. (1987)
18	1983-11-12	4.1	24	12.2	V	0.015	Weidenschilling et al. (1987)
19	1983-11-14	5.8	14	11.8	V	0.024	Weidenschilling et al. (1987)
20	1983-12-28	6.0	83	8.1	V	0.068	Barucci (1983)
21	1983-12-29	0.8	15	8.2	V	0.032	Barucci (1983)
22	1983-12-30	4.0	77	8.4	V	0.047	Barucci (1983)
23	1984-02-21	4.8	34	18.1	V	0.028	Weidenschilling et al. (1987)
24	1985-01-18	2.2	21	25.8	V	0.020	Weidenschilling et al. (1987)
25	1985-01-19	3.9	21	25.7	V	0.023	Weidenschilling et al. (1987)
26	1985-04-11	5.1	13	5.8	V	0.014	Weidenschilling et al. (1987)
27	1987-10-17	5.8	25	8.7	V	0.019	Weidenschilling et al. (1987)
28	1988-12-20	5.9	37	11.5	V	0.042	Weidenschilling et al. (1987)
29	1988-12-21	5.8	15	11.2	V	0.035	Weidenschilling et al. (1987)
30	2001-11-21	7.2	103	5.4	V	0.023	L. Bernasconi
31	2001-11-22	8.4	107	5.4	V	0.023	L. Bernasconi
32	2001-11-23	7.0	102	5.5	V	0.027	L. Bernasconi
33	2001-11-24	8.8	87	5.5	V	0.022	L. Bernasconi
34	2008-06-25	2.3	49	12.9	clear	0.018	SuperWASP - J. Grice
35	2009-10-16	3.0	45	4.3	clear	0.021	SuperWASP - J. Grice
36	2009-09-25	2.7	117	8.2	V	0.019	ASTEP
37	2009-10-16	2.8	34	11.2	clear	0.015	SuperWASP - J. Grice
38	2017-01-08	2.3	31	22.0	R	0.024	Vachier, Klotz, Teng, Peyrot, Thierry, Berthier
39	2018-07-09	10.6	651	19.1	R	0.023	E. Jehin
40	2018-07-10	6.0	507	18.9	R	0.024	E. Jehin
41	2018-08-03	3.6	200	12.4	R	0.023	S. Fauvau
42	2018-08-04	6.2	200	12.1	R	0.020	S. Fauvau
43	2018-08-05	2.1	200	11.7	R	0.019	S. Fauvau
44	2018-08-05	1.9	137	11.4	R	0.013	S. Fauvau
45	2018-08-06	1.8	136	11.1	R	0.012	S. Fauvau
46	2018-08-11	1.6	139	9.3	R	0.009	S. Fauvau
47	2018-08-14	1.8	139	8.2	R	0.008	S. Fauvau
48	2018-08-15	1.4	105	7.8	R	0.007	S. Fauvau
49	2018-11-19	3.1	52	18.6	R	0.016	Vachier, Klotz, Teng, Peyrot, Thierry, Berthier

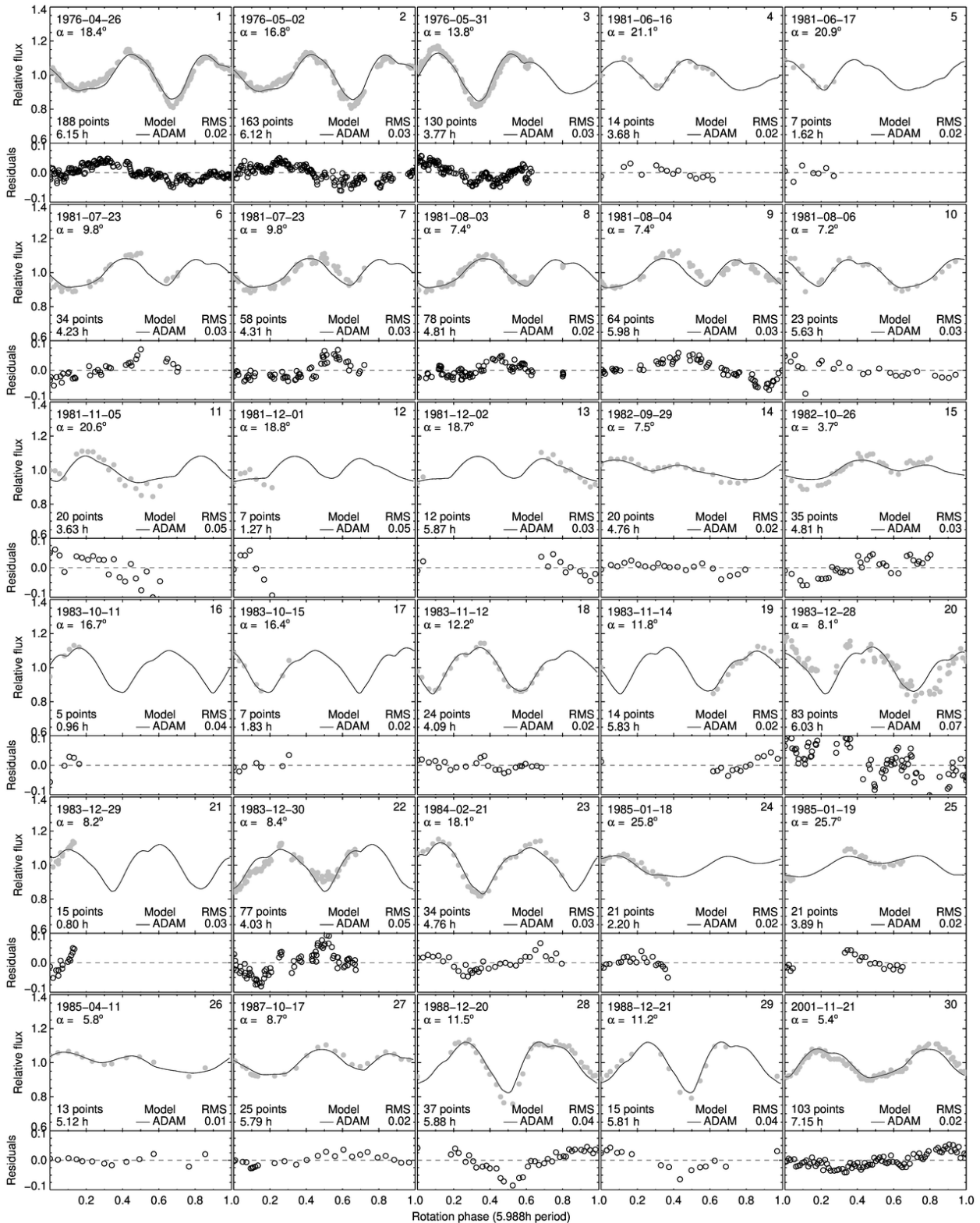


Fig. B.3: The optical lightcurves of Daphne (grey spheres), compared with the synthetic lightcurves generated with the shape model (black lines). On each panel, the observing date, number of points, duration of the lightcurve (in hours), and RMS residuals between the observations and the synthetic lightcurves are displayed. Measurement uncertainties are seldom provided by the observers but can be estimated from the spread of measurements.

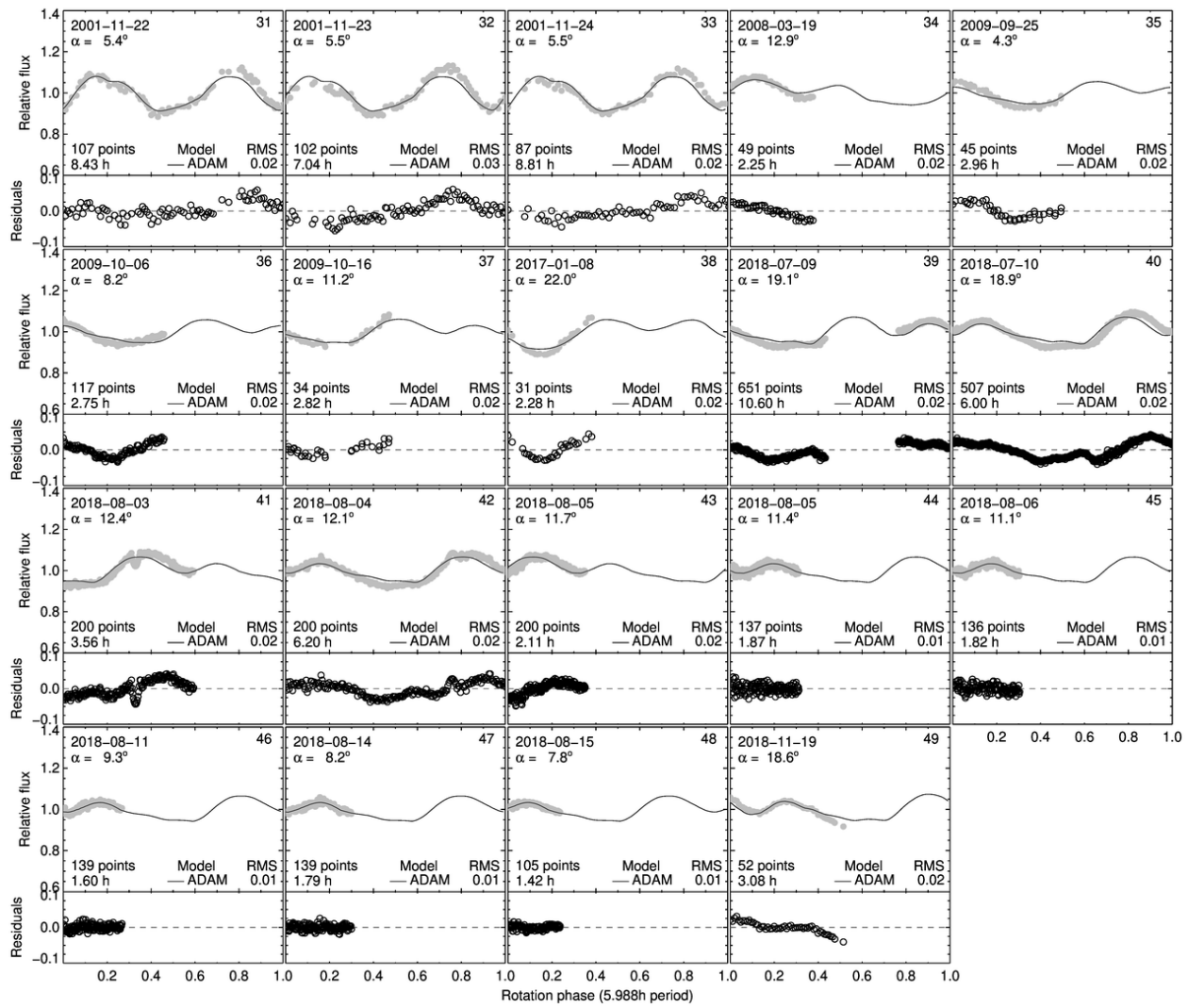


Fig. B.3: Cont'd

Appendix C: Magnitude and position of the satellite

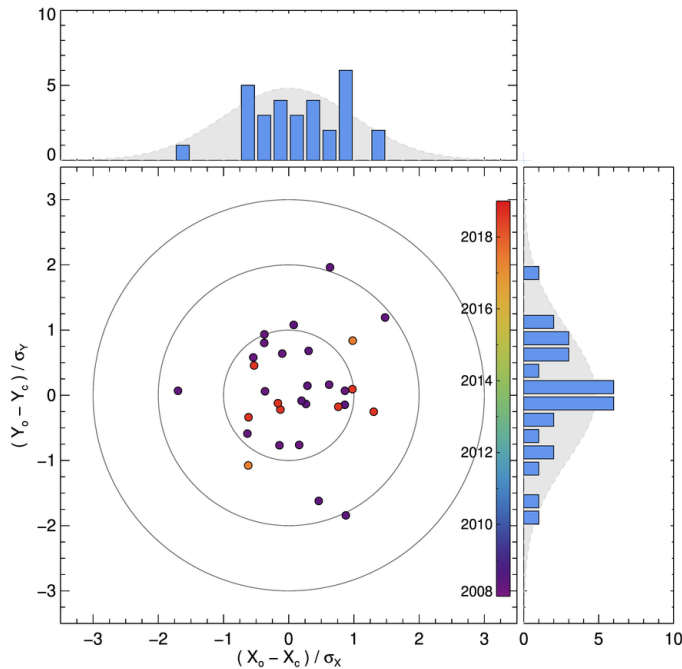


Fig. C.1: Distribution of residuals for the satellite between the observed (index o) and predicted (index c) positions, normalized by the uncertainty on the measured positions (σ), and color-coded by observing epoch. X stands for right ascension and Y for declination. The three large gray circles represent the 1, 2, and 3 σ limits (typically 10 mas at 1 σ). The top panel shows the histogram of residuals along X, and the right panel the residuals along Y. The light gray Gaussian in the background has a standard deviation of one.

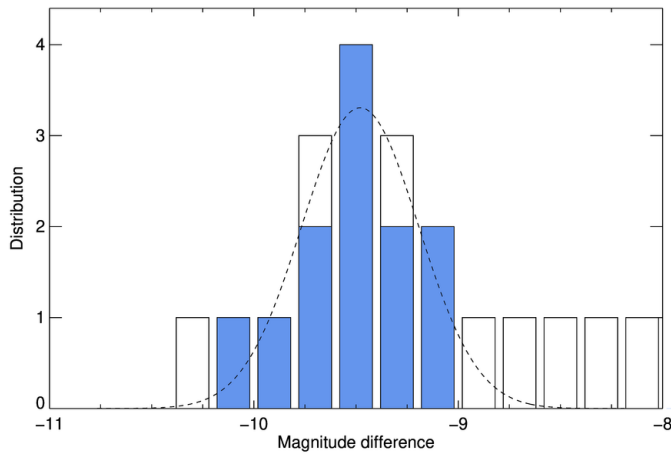


Fig. C.2: Distribution of the magnitude differences between Daphne and its satellite. The open bars represent all measurements, and the blue bars those more precise than 0.75 magnitude. The dashed black line represents the normal distribution fit to our results, with a mean and standard deviation of 9.49 ± 0.32 .

Table C.1: Astrometry of the satellite of Daphne. Date, mid-observing time (UTC), telescope, camera, filter, astrometry (X is aligned with Right Ascension, and Y with Declination, and o and c indices stand for observed and computed positions), and photometry (magnitude difference ΔM with uncertainty δM).

Date	UTC	Tel.	Cam.	Filter	X_o (mas)	Y_o (mas)	X_{o-c} (mas)	Y_{o-c} (mas)	σ (mas)	ΔM (mag)	δM (mag)
2008-03-28	12:05:30.1	Keck	NIRC2	J	-554	60	-6	-5	9.94	-9.59	0.85
2008-03-28	12:07:59.5	Keck	NIRC2	J	-549	53	-1	-7	9.94	-10.06	0.64
2008-03-28	12:56:28.9	Keck	NIRC2	H	-531	-19	-5	5	9.94	—	—
2008-03-28	13:45:16.2	Keck	NIRC2	H	-476	-110	8	0	9.94	—	—
2008-03-28	13:48:16.8	Keck	NIRC2	H	-475	-115	6	1	9.94	-9.70	0.14
2008-03-28	14:09:03.8	Keck	NIRC2	H	-457	-160	1	-7	9.94	-9.10	2.19
2008-03-28	14:30:11.3	Keck	NIRC2	H	-435	-187	-3	0	9.94	—	—
2008-03-28	14:53:08.0	Keck	NIRC2	K _p	-403	-215	-3	9	9.94	-9.84	0.73
2008-03-28	14:57:06.5	Keck	NIRC2	K _p	-397	-222	-3	7	9.94	—	—
2008-03-28	15:00:34.9	Keck	NIRC2	H	-389	-229	0	6	9.94	—	—
2008-04-23	12:17:26.4	Keck	NIRC2	H	-424	376	-16	0	9.94	—	—
2008-04-23	12:53:37.9	Keck	NIRC2	H	-453	361	6	19	9.94	—	—
2008-04-23	12:58:51.4	Keck	NIRC2	H	-452	347	14	11	9.94	—	—
2008-05-10	02:43:04.5	VLT	NACO	H	550	-177	3	-1	13.24	-9.56	0.78
2008-05-10	02:47:42.2	VLT	NACO	H	552	-167	3	1	13.24	-9.53	1.49
2008-05-10	03:14:05.9	VLT	NACO	H	559	-124	4	9	13.24	-9.52	0.84
2008-05-10	03:18:44.1	VLT	NACO	H	556	-112	1	14	13.24	-9.29	1.13
2008-05-14	02:20:19.1	VLT	NACO	H	-516	142	11	-24	13.24	-9.28	0.37
2008-05-14	02:24:59.4	VLT	NACO	H	-523	139	6	-21	13.24	-9.02	0.19
2008-05-27	02:44:38.8	VLT	NACO	H	449	-256	11	-1	13.24	—	—
2008-05-27	02:49:12.7	VLT	NACO	H	445	-251	2	-1	13.24	-9.68	0.65
2017-05-05	22:51:25.1	VLT	IFS	YJH	404	158	-6	-10	10.00	—	—
2017-05-20	01:01:27.4	VLT	ZIMPOL	R	-360	35	9	8	10.00	—	—
2018-08-06	06:28:30.9	VLT	ZIMPOL	R	-268	208	-5	4	10.00	—	—
2018-08-06	06:33:09.9	VLT	ZIMPOL	R	-266	203	-6	-3	10.00	—	—
2018-08-06	07:40:49.4	VLT	ZIMPOL	R	-193	244	7	-1	10.00	—	—
2018-08-06	07:45:25.2	VLT	ZIMPOL	R	-186	249	9	0	10.00	—	—
2018-08-06	07:59:15.8	VLT	ZIMPOL	R	-169	251	13	-2	10.00	-9.97	0.63
2018-08-06	09:20:18.1	VLT	ZIMPOL	R	-92	271	-1	-2	10.00	—	—
2018-08-06	09:24:57.2	VLT	ZIMPOL	R	-87	272	-1	-1	10.00	-10.02	1.34
					Average	2	0	15	-9.49	0.28	
					Standard deviation	7	9	2	0.32	0.18	

**Appendix D: Mass and diameter of Ch and Cgh
asteroids**

Table D.1: Dynamical class (IMB, MMB, and OMB stand for Inner, Middle, and Outer belt respectively), taxonomic class, mass (\mathcal{M}), diameter (\mathcal{D}), and density (ρ) of Ch/Cgh asteroids used in this work, compiled following the recipes described in [Carry \(2012\)](#). Individual diameter and mass estimates are listed in Tables D.2 and D.3.

#	Name	Dyn.	Taxo.	\mathcal{M} (kg)	$\sigma_{\mathcal{M}}$ (kg)	\mathcal{D} (km)	$\sigma_{\mathcal{D}}$ (km)	ρ (g·cm $^{-3}$)	σ_{ρ} (g·cm $^{-3}$)
13	Egeria	MMB	Ch	$8.42 \cdot 10^{18}$	$2.28 \cdot 10^{18}$	206.56	8.22	1.82	0.54
19	Fortuna	IMB	Ch	$9.03 \cdot 10^{18}$	$7.13 \cdot 10^{17}$	207.54	5.30	1.93	0.21
34	Circe	MMB	Ch	$4.16 \cdot 10^{18}$	$6.27 \cdot 10^{17}$	114.34	3.23	5.31	0.92
38	Leda	MMB	Cgh	$3.18 \cdot 10^{18}$	$5.97 \cdot 10^{17}$	118.62	4.22	3.64	0.79
41	Daphne	MMB	Ch	$6.10 \cdot 10^{18}$	$7.50 \cdot 10^{17}$	187.00	7.50	1.77	0.22
48	Doris	OMB	Ch	$7.71 \cdot 10^{18}$	$1.57 \cdot 10^{18}$	208.37	12.02	1.63	0.44
49	Pales	OMB	Ch	$4.10 \cdot 10^{18}$	$1.77 \cdot 10^{18}$	149.97	3.78	2.32	1.02
50	Virginia	MMB	Ch	$6.26 \cdot 10^{17}$	$2.06 \cdot 10^{17}$	88.51	4.65	1.72	0.63
51	Nemausa	IMB	Cgh	$2.62 \cdot 10^{18}$	$8.19 \cdot 10^{17}$	146.80	1.56	1.58	0.50
54	Alexandra	MMB	Cgh	$1.72 \cdot 10^{18}$	$5.89 \cdot 10^{17}$	150.12	8.14	0.97	0.37
58	Concordia	MMB	Ch	$1.28 \cdot 10^{17}$	$6.41 \cdot 10^{16}$	94.84	1.57	0.29	0.14
62	Erato	OMB	Ch	$1.38 \cdot 10^{17}$	$6.91 \cdot 10^{16}$	96.06	14.26	0.30	0.20
70	Panopaea	MMB	Cgh	$3.64 \cdot 10^{18}$	$5.94 \cdot 10^{17}$	135.34	5.47	2.81	0.57
78	Diana	MMB	Ch	$8.99 \cdot 10^{17}$	$5.31 \cdot 10^{17}$	125.33	4.77	0.87	0.53
84	Klio	IMB	Ch	$6.63 \cdot 10^{17}$	$1.51 \cdot 10^{17}$	78.76	1.12	2.59	0.60
91	Aegina	MMB	Ch	$6.07 \cdot 10^{17}$	$2.98 \cdot 10^{17}$	103.67	4.86	1.04	0.53
95	Arethusa	OMB	Ch	$4.18 \cdot 10^{18}$	$7.95 \cdot 10^{17}$	138.07	10.19	3.03	0.89
98	Ianthe	MMB	Ch	$8.53 \cdot 10^{17}$	$1.65 \cdot 10^{17}$	105.48	3.29	1.39	0.30
104	Klymene	OMB	Ch	$1.91 \cdot 10^{18}$	$6.59 \cdot 10^{17}$	130.48	5.85	1.64	0.61
105	Artemis	IMB	Ch	$1.43 \cdot 10^{18}$	$4.14 \cdot 10^{17}$	122.44	2.70	1.49	0.44
106	Dione	OMB	Cgh	$4.86 \cdot 10^{18}$	$2.18 \cdot 10^{18}$	146.60	3.41	2.95	1.34
109	Felicitas	MMB	Ch	$1.69 \cdot 10^{17}$	$3.50 \cdot 10^{16}$	82.38	5.09	0.58	0.16
111	Ate	MMB	Ch	$1.87 \cdot 10^{18}$	$3.48 \cdot 10^{17}$	134.28	2.08	1.48	0.28
112	Iphigenia	IMB	Ch	$4.52 \cdot 10^{17}$	$2.12 \cdot 10^{17}$	71.06	0.67	2.41	1.13
121	Hermione	Cybele	Ch	$4.94 \cdot 10^{18}$	$4.21 \cdot 10^{17}$	196.69	8.36	1.24	0.19
127	Johanna	MMB	Ch	$2.39 \cdot 10^{18}$	$9.97 \cdot 10^{17}$	120.04	0.05	2.64	1.10
130	Elektra	OMB	Ch	$6.20 \cdot 10^{18}$	$4.45 \cdot 10^{16}$	189.56	6.24	1.74	0.17
134	Sophrosyne	MMB	Ch	$9.52 \cdot 10^{17}$	$1.24 \cdot 10^{18}$	107.02	9.63	1.48	1.97
141	Lumen	MMB	Ch	$3.27 \cdot 10^{18}$	$9.33 \cdot 10^{17}$	132.24	1.73	2.70	0.78
144	Vibilia	MMB	Ch	$3.75 \cdot 10^{18}$	$6.95 \cdot 10^{17}$	141.86	1.42	2.51	0.47
145	Adeona	MMB	Ch	$2.32 \cdot 10^{18}$	$2.11 \cdot 10^{17}$	149.48	5.72	1.33	0.19
146	Lucina	MMB	Ch	$1.18 \cdot 10^{17}$	$5.91 \cdot 10^{16}$	129.10	3.94	0.10	0.05
156	Xanthippe	MMB	Ch	$1.28 \cdot 10^{18}$	$2.52 \cdot 10^{18}$	115.93	4.26	1.57	3.10
159	Aemilia	OMB	Ch	$4.18 \cdot 10^{18}$	$5.97 \cdot 10^{17}$	133.93	7.59	3.32	0.74
162	Laurentia	OMB	Ch	$3.36 \cdot 10^{17}$	$1.67 \cdot 10^{17}$	98.65	1.95	0.67	0.33
163	Erigone	IMB	Ch	$5.79 \cdot 10^{17}$	$2.43 \cdot 10^{17}$	72.29	1.22	2.93	1.24
168	Sibylla	Cybele	Ch	$5.75 \cdot 10^{18}$	$1.68 \cdot 10^{18}$	148.97	4.51	3.32	1.01
176	Iduna	OMB	Ch	$3.36 \cdot 10^{17}$	$1.68 \cdot 10^{17}$	119.40	3.57	0.38	0.19
187	Lamberta	MMB	Ch	$8.05 \cdot 10^{17}$	$7.07 \cdot 10^{17}$	131.18	1.21	0.68	0.60
195	Eurykleia	OMB	Ch	$1.44 \cdot 10^{17}$	$7.19 \cdot 10^{16}$	90.22	4.21	0.37	0.19
200	Dynamene	MMB	Ch	$1.29 \cdot 10^{18}$	$8.87 \cdot 10^{17}$	131.11	2.95	1.09	0.76
205	Martha	MMB	Ch	$1.19 \cdot 10^{17}$	$5.94 \cdot 10^{16}$	69.44	7.11	0.68	0.40
211	Isolda	OMB	Ch	$3.31 \cdot 10^{18}$	$1.27 \cdot 10^{18}$	151.33	4.77	1.83	0.72
238	Hypatia	OMB	Ch	$3.31 \cdot 10^{18}$	$9.25 \cdot 10^{17}$	144.90	2.21	2.08	0.59
266	Aline	MMB	Ch	$1.43 \cdot 10^{18}$	$6.93 \cdot 10^{17}$	104.96	4.95	2.36	1.19
303	Josephina	OMB	Ch	$1.31 \cdot 10^{17}$	$6.57 \cdot 10^{16}$	100.64	7.25	0.25	0.13
345	Tercidina	IMB	Ch	$1.17 \cdot 10^{18}$	$5.11 \cdot 10^{17}$	99.09	1.40	2.30	1.01
350	Ornamenta	OMB	Ch	$2.59 \cdot 10^{17}$	$1.29 \cdot 10^{17}$	111.97	8.43	0.35	0.19
356	Liguria	MMB	Ch	$2.62 \cdot 10^{18}$	$2.16 \cdot 10^{18}$	139.97	6.22	1.82	1.52
358	Apollonia	OMB	Ch	$1.60 \cdot 10^{17}$	$7.99 \cdot 10^{16}$	89.11	1.78	0.43	0.22
362	Havnia	MMB	Ch	$1.67 \cdot 10^{17}$	$8.36 \cdot 10^{16}$	89.09	3.97	0.45	0.23
366	Vincentina	OMB	Ch	$1.00 \cdot 10^{17}$	$5.00 \cdot 10^{16}$	87.73	3.54	0.28	0.15
373	Melusina	OMB	Ch	$3.43 \cdot 10^{17}$	$1.72 \cdot 10^{17}$	96.76	2.85	0.72	0.37
377	Campania	MMB	Ch	$1.52 \cdot 10^{17}$	$7.61 \cdot 10^{16}$	92.40	1.08	0.37	0.18

Table D.1: continued.

#	Name	Dyn.	Taxo.	\mathcal{M} (kg)	$\delta\mathcal{M}$ (kg)	\mathcal{D} (km)	$\delta\mathcal{D}$ (km)	ρ (g·cm ⁻³)	$\delta\rho$ (g·cm ⁻³)
404	Arsinoe	MMB	Ch	$8.21 \cdot 10^{17}$	$1.70 \cdot 10^{17}$	95.78	3.10	1.78	0.41
405	Thia	MMB	Ch	$1.68 \cdot 10^{18}$	$6.79 \cdot 10^{17}$	119.36	7.70	1.89	0.85
407	Arachne	MMB	Ch	$1.26 \cdot 10^{17}$	$6.28 \cdot 10^{16}$	97.33	1.16	0.26	0.13
410	Chloris	MMB	Ch	$1.89 \cdot 10^{18}$	$5.95 \cdot 10^{17}$	111.18	7.35	2.63	0.98
442	Eichsfeldia	IMB	Ch	$2.50 \cdot 10^{17}$	$1.23 \cdot 10^{17}$	65.30	1.65	1.71	0.85
445	Edna	OMB	Ch	$1.24 \cdot 10^{18}$	$6.10 \cdot 10^{17}$	88.11	2.18	3.46	1.72
481	Emita	MMB	Ch	$1.31 \cdot 10^{18}$	$6.24 \cdot 10^{17}$	107.74	5.40	2.00	1.00
488	Kreusa	OMB	Ch	$2.47 \cdot 10^{18}$	$4.25 \cdot 10^{17}$	167.51	6.56	1.00	0.21
490	Veritas	OMB	Ch	$2.02 \cdot 10^{18}$	$9.87 \cdot 10^{17}$	114.87	3.64	2.55	1.27
503	Evelyn	MMB	Ch	$8.28 \cdot 10^{17}$	$3.85 \cdot 10^{17}$	89.48	2.49	2.21	1.04
521	Brixia	MMB	Ch	$4.10 \cdot 10^{17}$	$2.09 \cdot 10^{17}$	118.11	6.86	0.47	0.26
554	Peraga	IMB	Ch	$5.86 \cdot 10^{17}$	$2.18 \cdot 10^{17}$	96.65	1.19	1.24	0.46
602	Marianna	OMB	Ch	$3.20 \cdot 10^{18}$	$1.36 \cdot 10^{18}$	127.54	2.55	2.95	1.26
654	Zelinda	IMB	Ch	$1.22 \cdot 10^{18}$	$3.51 \cdot 10^{17}$	125.90	4.49	1.17	0.36
694	Ekard	MMB	Ch	$1.20 \cdot 10^{17}$	$5.94 \cdot 10^{16}$	93.95	4.82	0.28	0.14
735	Marghanna	MMB	Ch	$7.23 \cdot 10^{17}$	$2.98 \cdot 10^{17}$	71.75	2.11	3.74	1.58
751	Faina	MMB	Ch	$3.67 \cdot 10^{18}$	$6.38 \cdot 10^{17}$	106.86	1.15	5.74	1.02
776	Berbericia	OMB	Cgh	$4.46 \cdot 10^{18}$	$4.16 \cdot 10^{18}$	150.92	3.20	2.48	2.31
788	Hohensteina	OMB	Ch	$1.85 \cdot 10^{17}$	$9.22 \cdot 10^{16}$	114.68	6.38	0.23	0.12
791	Ani	OMB	Ch	$1.47 \cdot 10^{17}$	$7.37 \cdot 10^{16}$	99.20	4.96	0.29	0.15
914	Palisana	IMB	Ch	$4.89 \cdot 10^{17}$	$2.29 \cdot 10^{17}$	78.71	2.64	1.92	0.92
1467	Mashona	Cybele	Ch	$2.04 \cdot 10^{17}$	$1.02 \cdot 10^{17}$	95.08	1.30	0.45	0.23

Table D.2: The diameter estimates (\mathcal{D}) for all the Ch/Cgh asteroids available in the literature. For each, the 3σ uncertainty, method, and bibliographic reference are reported. The methods are IM-TE: Ellipsoid from Imaging, LCIMG: 3-D Model scaled with Imaging, ADAM & KOALA: Multidata 3-D Modeling, occ: Stellar Occultations, STM: Standard Thermal Model, NEATM: Near-Earth Asteroid Thermal Model, and TPM: Thermophysical Model.

#	Name	\mathcal{D} (km)	$\delta\mathcal{D}$ (km)	Method	Reference
13	Egeria	244.0	73.2	STM	Morrison & Zellner (2007)
13	Egeria	207.6	24.9	STM	Tedesco et al. (2004b)
13	Egeria	203.1	5.9	occ	Dunham et al. (2017)
13	Egeria	223.1	10.4	STM	Ryan & Woodward (2010)
13	Egeria	226.1	28.5	NEATM	Ryan & Woodward (2010)
13	Egeria	203.4	7.7	STM	Usui et al. (2011)
13	Egeria	227.0	77.9	NEATM	Masiero et al. (2011)
13	Egeria	202.6	150.2	NEATM	Nugent et al. (2015)
13	Egeria	209.0	24.0	ADAM	Hanuš et al. (2017b)
13	Egeria	201.0	12.0	ADAM	Hanuš et al. (2017b)
19	Fortuna	221.0	66.3	STM	Morrison & Zellner (2007)
19	Fortuna	210.1	11.3	occ	Dunham et al. (2017)
19	Fortuna	209.6	14.9	IM-TE	Drummond et al. (2011)
19	Fortuna	199.7	9.1	TPM	Usui et al. (2011)
19	Fortuna	223.0	130.8	NEATM	Masiero et al. (2011)
19	Fortuna	209.8	6.6	NEATM	Masiero et al. (2012)
19	Fortuna	187.0	39.0	LCIMG	Hanuš et al. (2013b)
19	Fortuna	211.0	12.0	ADAM	Hanuš et al. (2017b)
34	Circe	111.0	33.3	STM	Morrison & Zellner (2007)
34	Circe	113.5	9.9	STM	Tedesco et al. (2004b)
34	Circe	109.5	5.4	occ	Dunham et al. (2017)
34	Circe	97.4	8.5	STM	Ryan & Woodward (2010)
34	Circe	121.5	21.3	NEATM	Ryan & Woodward (2010)
34	Circe	96.0	30.0	LCOCC	Ďurech et al. (2011)
34	Circe	107.0	30.0	LCOCC	Ďurech et al. (2011)
34	Circe	116.5	3.4	STM	Usui et al. (2011)
34	Circe	113.2	8.7	NEATM	Masiero et al. (2011)
34	Circe	133.0	3.1	NEATM	Masiero et al. (2012)
34	Circe	117.0	42.0	LCIMG	Hanuš et al. (2013b)
34	Circe	116.0	33.0	LCIMG	Hanuš et al. (2013b)
34	Circe	114.1	131.3	NEATM	Nugent et al. (2015)
38	Leda	115.9	6.3	STM	Tedesco et al. (2004b)
38	Leda	97.3	8.1	STM	Ryan & Woodward (2010)
38	Leda	118.1	16.0	NEATM	Ryan & Woodward (2010)
38	Leda	114.2	4.6	STM	Usui et al. (2011)
38	Leda	116.0	46.5	NEATM	Masiero et al. (2011)
38	Leda	122.5	3.7	NEATM	Masiero et al. (2012)
38	Leda	114.2	84.6	NEATM	Nugent et al. (2015)
41	Daphne	203.0	60.9	STM	Morrison & Zellner (2007)
41	Daphne	174.0	35.1	STM	Tedesco et al. (2004b)
41	Daphne	172.4	12.2	STM	Ryan & Woodward (2010)
41	Daphne	207.9	31.6	NEATM	Ryan & Woodward (2010)
41	Daphne	187.0	60.0	LCOCC	Ďurech et al. (2011)
41	Daphne	201.5	22.5	TPM	Matter et al. (2011)
41	Daphne	185.5	10.5	TPM	Matter et al. (2011)
41	Daphne	179.6	7.7	STM	Usui et al. (2011)
41	Daphne	205.5	5.6	NEATM	Masiero et al. (2012)
41	Daphne	186.0	81.0	LCIMG	Hanuš et al. (2013b)
41	Daphne	198.7	185.1	NEATM	Nugent et al. (2015)
41	Daphne	188.0	15.0	ADAM	Hanuš et al. (2017b)
41	Daphne	187.0	27.9	KOALA	This work
48	Doris	221.8	22.5	STM	Tedesco et al. (2004b)
48	Doris	196.3	47.3	occ	Dunham et al. (2017)
48	Doris	211.3	48.0	STM	Ryan & Woodward (2010)
48	Doris	238.8	27.6	NEATM	Ryan & Woodward (2010)
48	Doris	200.3	8.2	STM	Usui et al. (2011)

Table D.2: continued.

#	Name (km)	\mathcal{D} (km)	$\delta\mathcal{D}$	Method	Reference
48	Doris	223.4	12.5	NEATM	Masiero et al. (2011)
48	Doris	165.4	125.4	NEATM	Nugent et al. (2015)
49	Pales	149.8	11.4	STM	Tedesco et al. (2004b)
49	Pales	157.5	14.7	STM	Ryan & Woodward (2010)
49	Pales	169.7	27.9	NEATM	Ryan & Woodward (2010)
49	Pales	148.0	7.7	STM	Usui et al. (2011)
49	Pales	166.2	6.5	NEATM	Masiero et al. (2012)
49	Pales	149.3	142.6	NEATM	Nugent et al. (2015)
49	Pales	138.8	124.6	NEATM	Nugent et al. (2015)
50	Virginia	99.8	15.6	STM	Tedesco et al. (2004b)
50	Virginia	99.0	9.1	NEATM	Ryan & Woodward (2010)
50	Virginia	84.4	2.5	STM	Usui et al. (2011)
50	Virginia	100.0	22.8	NEATM	Masiero et al. (2011)
50	Virginia	87.0	2.8	NEATM	Masiero et al. (2012)
51	Nemausa	151.0	45.3	STM	Morrison & Zellner (2007)
51	Nemausa	147.9	7.2	STM	Tedesco et al. (2004b)
51	Nemausa	155.9	11.9	STM	Ryan & Woodward (2010)
51	Nemausa	147.2	5.1	STM	Usui et al. (2011)
51	Nemausa	142.6	37.5	NEATM	Masiero et al. (2011)
51	Nemausa	146.1	248.9	NEATM	Masiero et al. (2012)
51	Nemausa	144.0	9.0	ADAM	Hanuš et al. (2017b)
54	Alexandra	175.0	52.5	STM	Morrison & Zellner (2007)
54	Alexandra	165.8	10.2	STM	Tedesco et al. (2004b)
54	Alexandra	147.0	7.0	OCC	Dunham et al. (2017)
54	Alexandra	177.4	13.7	STM	Ryan & Woodward (2010)
54	Alexandra	177.7	22.7	NEATM	Ryan & Woodward (2010)
54	Alexandra	135.0	60.0	LCOCC	Ďurech et al. (2011)
54	Alexandra	142.0	27.0	LCOCC	Ďurech et al. (2011)
54	Alexandra	144.5	5.4	STM	Usui et al. (2011)
54	Alexandra	142.0	44.3	NEATM	Masiero et al. (2011)
54	Alexandra	160.1	5.6	NEATM	Masiero et al. (2012)
54	Alexandra	128.0	33.0	LCIMG	Hanuš et al. (2013b)
54	Alexandra	143.0	15.0	ADAM	Hanuš et al. (2017b)
58	Concordia	93.4	9.0	STM	Tedesco et al. (2004b)
58	Concordia	93.6	3.2	NEATM	Usui et al. (2011)
58	Concordia	94.6	9.3	STM	Ryan & Woodward (2010)
58	Concordia	102.7	23.3	NEATM	Ryan & Woodward (2010)
58	Concordia	92.3	4.6	NEATM	Masiero et al. (2011)
58	Concordia	106.5	2.2	NEATM	Masiero et al. (2012)
58	Concordia	88.4	72.8	NEATM	Nugent et al. (2015)
58	Concordia	95.8	3.9	OCC	Dunham et al. (2017)
58	Concordia	96.0	2.5	OCC	Dunham et al. (2017)
62	Erato	95.4	6.0	STM	Tedesco et al. (2004b)
62	Erato	78.6	2.7	NEATM	Usui et al. (2011)
62	Erato	80.7	6.3	STM	Ryan & Woodward (2010)
62	Erato	105.6	16.1	NEATM	Ryan & Woodward (2010)
62	Erato	106.9	2.0	NEATM	Masiero et al. (2012)
62	Erato	82.3	71.1	NEATM	Nugent et al. (2015)
62	Erato	59.4	77.1	NEATM	Nugent et al. (2015)
70	Panopaea	151.0	45.3	STM	Morrison & Zellner (2007)
70	Panopaea	122.2	6.9	STM	Tedesco et al. (2004b)
70	Panopaea	105.2	8.4	STM	Ryan & Woodward (2010)
70	Panopaea	130.9	19.6	NEATM	Ryan & Woodward (2010)
70	Panopaea	131.2	4.5	OCC	Dunham et al. (2017)
70	Panopaea	141.4	5.7	STM	Usui et al. (2011)
70	Panopaea	139.0	11.5	NEATM	Masiero et al. (2011)
70	Panopaea	162.6	3.8	NEATM	Masiero et al. (2012)
70	Panopaea	115.3	127.5	NEATM	Nugent et al. (2015)
78	Diana	120.6	8.1	STM	Tedesco et al. (2004b)

Table D.2: continued.

#	Name (km)	\mathcal{D} (km)	$\delta\mathcal{D}$	Method	Reference
78	Diana	131.2	10.5	occ	Dunham et al. (2017)
78	Diana	116.0	14.5	STM	Ryan & Woodward (2010)
78	Diana	130.8	22.0	NEATM	Ryan & Woodward (2010)
78	Diana	126.5	5.0	STM	Usui et al. (2011)
78	Diana	179.3	146.2	NEATM	Masiero et al. (2012)
78	Diana	160.1	137.1	NEATM	Nugent et al. (2015)
84	Klio	87.0	26.1	STM	Morrison & Zellner (2007)
84	Klio	79.2	4.8	STM	Tedesco et al. (2004b)
84	Klio	68.1	6.5	STM	Ryan & Woodward (2010)
84	Klio	81.1	10.3	NEATM	Ryan & Woodward (2010)
84	Klio	78.3	2.9	STM	Usui et al. (2011)
84	Klio	79.0	14.6	NEATM	Masiero et al. (2011)
91	Aegina	104.0	31.2	STM	Morrison & Zellner (2007)
91	Aegina	109.8	9.9	STM	Tedesco et al. (2004b)
91	Aegina	111.6	6.3	occ	Dunham et al. (2017)
91	Aegina	100.2	3.7	NEATM	Usui et al. (2011)
91	Aegina	123.1	38.7	NEATM	Ryan & Woodward (2010)
91	Aegina	104.7	9.3	NEATM	Masiero et al. (2011)
91	Aegina	102.7	5.7	NEATM	Masiero et al. (2011)
91	Aegina	98.4	111.5	NEATM	Nugent et al. (2015)
95	Arethusa	229.0	68.7	STM	Morrison & Zellner (2007)
95	Arethusa	136.0	30.3	STM	Tedesco et al. (2004b)
95	Arethusa	131.1	8.7	occ	Dunham et al. (2017)
95	Arethusa	157.9	10.2	occ	Dunham et al. (2017)
95	Arethusa	135.1	4.8	occ	Dunham et al. (2017)
95	Arethusa	118.3	14.1	STM	Ryan & Woodward (2010)
95	Arethusa	139.5	21.3	NEATM	Ryan & Woodward (2010)
95	Arethusa	143.8	14.7	STM	Usui et al. (2011)
95	Arethusa	152.4	15.3	STM	Masiero et al. (2011)
95	Arethusa	147.9	14.7	STM	Masiero et al. (2011)
95	Arethusa	133.4	118.4	NEATM	Nugent et al. (2015)
98	Ianthe	104.4	5.4	STM	Tedesco et al. (2004b)
98	Ianthe	102.0	11.0	STM	Ryan & Woodward (2010)
98	Ianthe	114.3	15.7	NEATM	Ryan & Woodward (2010)
98	Ianthe	104.2	3.9	STM	Usui et al. (2011)
98	Ianthe	110.9	7.0	NEATM	Masiero et al. (2011)
98	Ianthe	132.8	3.4	NEATM	Masiero et al. (2012)
104	Klymene	123.7	9.3	STM	Tedesco et al. (2004b)
104	Klymene	109.9	11.5	STM	Ryan & Woodward (2010)
104	Klymene	131.2	19.9	NEATM	Ryan & Woodward (2010)
104	Klymene	126.5	5.6	STM	Usui et al. (2011)
104	Klymene	125.8	7.9	STM	Masiero et al. (2011)
104	Klymene	136.6	4.6	STM	Masiero et al. (2012)
104	Klymene	124.6	110.9	NEATM	Nugent et al. (2015)
105	Artemis	126.0	37.8	STM	Morrison & Zellner (2007)
105	Artemis	103.7	15.8	STM	Tedesco et al. (2004b)
105	Artemis	119.1	8.4	STM	Ryan & Woodward (2010)
105	Artemis	101.1	8.4	NEATM	Ryan & Woodward (2010)
105	Artemis	123.5	4.5	STM	Usui et al. (2011)
105	Artemis	119.0	52.0	NEATM	Masiero et al. (2011)
105	Artemis	112.8	102.1	NEATM	Masiero et al. (2012)
105	Artemis	112.8	105.7	NEATM	Nugent et al. (2015)
105	Artemis	94.9	69.7	NEATM	Nugent et al. (2015)
106	Dione	140.0	42.0	STM	Morrison & Zellner (2007)
106	Dione	145.6	2.5	occ	Dunham et al. (2017)
106	Dione	146.6	8.4	STM	Tedesco et al. (2004b)
106	Dione	127.3	10.1	STM	Ryan & Woodward (2010)
106	Dione	162.9	23.6	NEATM	Ryan & Woodward (2010)
106	Dione	153.4	7.1	STM	Usui et al. (2011)
106	Dione	207.9	6.5	NEATM	Masiero et al. (2012)

Table D.2: continued.

#	Name (km)	\mathcal{D} (km)	$\delta\mathcal{D}$	Method	Reference
106	Dione	83.4	2.5	NEATM	Grav et al. (2012)
106	Dione	89.2	101.9	NEATM	Nugent et al. (2015)
106	Dione	138.8	137.5	NEATM	Nugent et al. (2015)
106	Dione	151.7	77.7	NEATM	Ryan et al. (2015)
106	Dione	168.9	86.4	NEATM	Ryan et al. (2015)
106	Dione	182.9	93.5	NEATM	Ryan et al. (2015)
109	Felicitas	75.0	22.5	STM	Morrison & Zellner (2007)
109	Felicitas	89.4	7.5	STM	Tedesco et al. (2004b)
109	Felicitas	88.2	2.4	OCC	Dunham et al. (2017)
109	Felicitas	79.5	7.3	STM	Ryan & Woodward (2010)
109	Felicitas	111.4	27.4	NEATM	Ryan & Woodward (2010)
109	Felicitas	80.8	3.7	STM	Usui et al. (2011)
109	Felicitas	89.0	18.5	STM	Masiero et al. (2011)
109	Felicitas	99.9	3.0	STM	Masiero et al. (2012)
109	Felicitas	67.5	2.0	NEATM	Grav et al. (2012)
109	Felicitas	92.4	94.6	NEATM	Nugent et al. (2015)
109	Felicitas	64.7	71.5	NEATM	Nugent et al. (2015)
109	Felicitas	94.6	85.2	NEATM	Nugent et al. (2015)
111	Ate	134.6	13.8	STM	Tedesco et al. (2004b)
111	Ate	119.0	19.2	OCC	Dunham et al. (2017)
111	Ate	130.4	2.7	OCC	Dunham et al. (2017)
111	Ate	134.9	1.2	OCC	Dunham et al. (2017)
111	Ate	140.2	7.2	STM	Ryan & Woodward (2010)
111	Ate	153.2	17.4	NEATM	Ryan & Woodward (2010)
111	Ate	146.6	7.0	STM	Usui et al. (2011)
111	Ate	135.0	55.7	NEATM	Masiero et al. (2011)
112	Iphigenia	72.2	13.2	STM	Tedesco et al. (2004b)
112	Iphigenia	59.8	6.2	STM	Ryan & Woodward (2010)
112	Iphigenia	80.6	12.7	NEATM	Ryan & Woodward (2010)
112	Iphigenia	71.1	2.8	STM	Usui et al. (2011)
112	Iphigenia	70.4	8.7	NEATM	Masiero et al. (2011)
112	Iphigenia	84.9	68.6	NEATM	Masiero et al. (2012)
112	Iphigenia	69.6	64.6	NEATM	Nugent et al. (2015)
112	Iphigenia	70.3	52.9	NEATM	Nugent et al. (2015)
121	Hermione	209.0	14.1	STM	Tedesco et al. (2004b)
121	Hermione	178.9	21.6	IM	Marchis et al. (2005)
121	Hermione	138.8	35.7	IM	Marchis et al. (2005)
121	Hermione	189.0	21.0	IM	Marchis et al. (2006)
121	Hermione	187.0	18.0	KOALA	Descamps et al. (2009)
121	Hermione	221.6	17.9	STM	Ryan & Woodward (2010)
121	Hermione	212.0	23.1	NEATM	Ryan & Woodward (2010)
121	Hermione	194.1	8.1	STM	Usui et al. (2011)
121	Hermione	165.0	13.5	NEATM	Masiero et al. (2011)
121	Hermione	192.4	22.1	NEATM	Marchis et al. (2012)
121	Hermione	220.0	66.0	TPM	Marchis et al. (2012)
121	Hermione	201.1	190.3	NEATM	Nugent et al. (2015)
121	Hermione	155.3	158.8	NEATM	Nugent et al. (2015)
127	Johanna	123.3	13.1	STM	Tedesco et al. (2004a)
127	Johanna	113.0	26.4	OCC	Dunham et al. (2017)
127	Johanna	109.6	0.0	STM	Ryan & Woodward (2010)
127	Johanna	120.0	0.0	NEATM	Ryan & Woodward (2010)
127	Johanna	114.2	4.6	TPM	Usui et al. (2011)
127	Johanna	129.1	3.0	NEATM	Masiero et al. (2012)
127	Johanna	108.0	30.0	LCOCC	Marciniak et al. (2012)
127	Johanna	116.0	30.0	LCOCC	Marciniak et al. (2012)
127	Johanna	106.4	127.9	NEATM	Nugent et al. (2015)
130	Elektra	174.0	52.2	STM	Morrison & Zellner (2007)
130	Elektra	182.2	35.4	STM	Tedesco et al. (2004b)
130	Elektra	191.0	6.0	IM	Marchis et al. (2006)
130	Elektra	196.0	33.0	NEATM	Marchis et al. (2008b)

Table D.2: continued.

#	Name (km)	\mathcal{D} (km)	$\delta\mathcal{D}$	Method	Reference
130	Elektra	215.0	45.0	IM	Marchis et al. (2008b)
130	Elektra	158.8	18.3	STM	Ryan & Woodward (2010)
130	Elektra	200.5	40.0	NEATM	Ryan & Woodward (2010)
130	Elektra	191.0	42.0	LCOCC	Ďurech et al. (2011)
130	Elektra	183.0	6.8	STM	Usui et al. (2011)
130	Elektra	198.9	12.3	NEATM	Masiero et al. (2011)
130	Elektra	161.9	11.5	NEATM	Masiero et al. (2012)
130	Elektra	201.2	25.5	NEATM	Marchis et al. (2012)
130	Elektra	197.0	60.0	TPM	Marchis et al. (2012)
130	Elektra	185.0	60.0	LCIMG	Hanuš et al. (2013b)
130	Elektra	158.9	138.0	NEATM	Nugent et al. (2015)
130	Elektra	199.0	21.0	ADAM	Hanuš et al. (2017a)
134	Sophrosyne	123.3	6.0	STM	Tedesco et al. (2004b)
134	Sophrosyne	186.1	57.0	OCC	Dunham et al. (2017)
134	Sophrosyne	122.9	14.7	STM	Ryan & Woodward (2010)
134	Sophrosyne	127.2	18.7	NEATM	Ryan & Woodward (2010)
134	Sophrosyne	100.4	4.0	STM	Usui et al. (2011)
134	Sophrosyne	112.2	32.4	STM	Masiero et al. (2011)
134	Sophrosyne	104.5	3.8	STM	Masiero et al. (2012)
141	Lumen	120.4	13.7	STM	Tedesco et al. (2004a)
141	Lumen	131.0	8.7	STM	Tedesco et al. (2004b)
141	Lumen	137.4	36.2	OCC	Dunham et al. (2017)
141	Lumen	110.9	9.8	STM	Ryan & Woodward (2010)
141	Lumen	139.8	23.7	NEATM	Ryan & Woodward (2010)
141	Lumen	132.2	4.5	STM	Usui et al. (2011)
141	Lumen	137.1	43.7	NEATM	Masiero et al. (2011)
144	Vibia	131.0	39.3	STM	Morrison & Zellner (2007)
144	Vibia	142.4	7.8	STM	Tedesco et al. (2004b)
144	Vibia	142.5	15.0	OCC	Dunham et al. (2017)
144	Vibia	138.4	27.4	STM	Ryan & Woodward (2010)
144	Vibia	161.2	27.1	NEATM	Ryan & Woodward (2010)
144	Vibia	142.2	5.3	STM	Usui et al. (2011)
144	Vibia	141.0	9.0	ADAM	Hanuš et al. (2017b)
144	Vibia	131.4	99.9	NEATM	Nugent et al. (2015)
145	Adeona	151.1	9.6	STM	Tedesco et al. (2004b)
145	Adeona	141.0	71.2	OCC	Dunham et al. (2017)
145	Adeona	126.0	10.8	STM	Ryan & Woodward (2010)
145	Adeona	157.9	22.7	NEATM	Ryan & Woodward (2010)
145	Adeona	141.4	15.5	STM	Usui et al. (2011)
145	Adeona	151.0	33.8	NEATM	Masiero et al. (2011)
145	Adeona	151.0	25.7	NEATM	Masiero et al. (2011)
145	Adeona	115.5	112.9	NEATM	Nugent et al. (2015)
146	Lucina	132.2	7.2	STM	Tedesco et al. (2004b)
146	Lucina	141.0	42.3	STM	Morrison & Zellner (2007)
146	Lucina	107.5	5.0	OCC	Dunham et al. (2017)
146	Lucina	134.0	48.0	OCC	Dunham et al. (2017)
146	Lucina	126.9	4.9	NEATM	Usui et al. (2011)
146	Lucina	128.0	14.0	STM	Ryan & Woodward (2010)
146	Lucina	144.7	24.8	NEATM	Ryan & Woodward (2010)
146	Lucina	131.8	14.4	NEATM	Masiero et al. (2011)
146	Lucina	160.3	3.6	NEATM	Masiero et al. (2012)
146	Lucina	113.1	88.9	NEATM	Nugent et al. (2015)
146	Lucina	119.0	33.0	LCIMG	Hanuš et al. (2013b)
156	Xanthippe	121.0	7.5	STM	Tedesco et al. (2004b)
156	Xanthippe	122.0	10.5	STM	Ryan & Woodward (2010)
156	Xanthippe	114.6	12.7	NEATM	Ryan & Woodward (2010)
156	Xanthippe	115.5	5.2	STM	Usui et al. (2011)
156	Xanthippe	110.7	6.6	NEATM	Masiero et al. (2011)
156	Xanthippe	143.4	2.7	NEATM	Masiero et al. (2012)
156	Xanthippe	122.0	95.0	NEATM	Nugent et al. (2015)

Table D.2: continued.

#	Name (km)	\mathcal{D} (km)	$\delta\mathcal{D}$	Method	Reference
156	Xanthippe	112.4	116.6	NEATM	Nugent et al. (2015)
159	Aemilia	140.0	42.0	STM	Morrison & Zellner (2007)
159	Aemilia	125.0	7.2	STM	Tedesco et al. (2004b)
159	Aemilia	141.7	4.5	OCC	Dunham et al. (2017)
159	Aemilia	123.3	15.3	STM	Ryan & Woodward (2010)
159	Aemilia	132.6	24.8	NEATM	Ryan & Woodward (2010)
159	Aemilia	130.0	6.9	STM	Usui et al. (2011)
159	Aemilia	127.4	8.1	STM	Masiero et al. (2011)
159	Aemilia	130.0	21.0	LCOCC	Marciniak et al. (2018)
159	Aemilia	138.0	21.0	LCOCC	Marciniak et al. (2018)
159	Aemilia	137.0	24.0	LCTPM	Marciniak et al. (2018)
162	Laurentia	99.1	7.8	STM	Tedesco et al. (2004b)
162	Laurentia	85.3	8.6	NEATM	Usui et al. (2011)
162	Laurentia	102.4	12.2	STM	Ryan & Woodward (2010)
162	Laurentia	106.4	18.0	NEATM	Ryan & Woodward (2010)
162	Laurentia	104.0	9.8	NEATM	Masiero et al. (2011)
162	Laurentia	101.3	3.2	NEATM	Masiero et al. (2012)
162	Laurentia	97.7	1.7	NEATM	Masiero et al. (2012)
162	Laurentia	97.2	11.1	OCC	Dunham et al. (2017)
163	Erigone	72.6	17.1	STM	Tedesco et al. (2004b)
163	Erigone	70.7	13.6	STM	Ryan & Woodward (2010)
163	Erigone	77.6	14.0	NEATM	Ryan & Woodward (2010)
163	Erigone	72.1	2.8	STM	Usui et al. (2011)
163	Erigone	81.6	9.2	NEATM	Masiero et al. (2011)
163	Erigone	69.7	59.8	NEATM	Nugent et al. (2015)
168	Sibylla	148.4	12.0	STM	Tedesco et al. (2004b)
168	Sibylla	154.6	6.0	STM	Ryan & Woodward (2010)
168	Sibylla	155.8	31.8	NEATM	Ryan & Woodward (2010)
168	Sibylla	146.5	5.2	STM	Usui et al. (2011)
168	Sibylla	144.0	8.6	NEATM	Masiero et al. (2011)
168	Sibylla	145.1	154.1	NEATM	Nugent et al. (2015)
168	Sibylla	141.8	92.5	NEATM	Nugent et al. (2015)
176	Iduna	121.0	6.6	STM	Tedesco et al. (2004b)
176	Iduna	119.5	3.9	NEATM	Usui et al. (2011)
176	Iduna	112.6	13.2	STM	Ryan & Woodward (2010)
176	Iduna	131.1	18.4	NEATM	Ryan & Woodward (2010)
176	Iduna	122.2	8.1	NEATM	Masiero et al. (2011)
176	Iduna	115.1	127.8	NEATM	Nugent et al. (2015)
176	Iduna	115.6	5.5	OCC	Dunham et al. (2017)
176	Iduna	126.9	12.6	OCC	Dunham et al. (2017)
187	Lamberta	130.4	8.1	STM	Tedesco et al. (2004b)
187	Lamberta	131.4	14.0	STM	Ryan & Woodward (2010)
187	Lamberta	132.1	23.2	NEATM	Ryan & Woodward (2010)
187	Lamberta	130.4	5.7	STM	Usui et al. (2011)
187	Lamberta	133.0	7.5	NEATM	Masiero et al. (2011)
187	Lamberta	147.3	4.2	NEATM	Masiero et al. (2012)
187	Lamberta	132.1	123.0	NEATM	Nugent et al. (2015)
187	Lamberta	125.2	137.1	NEATM	Nugent et al. (2015)
195	Eurykleia	85.7	5.1	STM	Tedesco et al. (2004b)
195	Eurykleia	89.4	3.3	NEATM	Usui et al. (2011)
195	Eurykleia	82.9	10.0	STM	Ryan & Woodward (2010)
195	Eurykleia	88.3	12.2	NEATM	Ryan & Woodward (2010)
195	Eurykleia	80.3	6.0	NEATM	Masiero et al. (2011)
195	Eurykleia	93.1	2.2	NEATM	Masiero et al. (2012)
195	Eurykleia	75.0	56.8	NEATM	Nugent et al. (2015)
195	Eurykleia	80.0	78.4	NEATM	Nugent et al. (2015)
200	Dynamene	128.4	6.3	STM	Tedesco et al. (2004b)
200	Dynamene	125.1	17.7	STM	Ryan & Woodward (2010)
200	Dynamene	135.9	20.7	NEATM	Ryan & Woodward (2010)
200	Dynamene	129.2	10.9	OCC	Dunham et al. (2017)

Table D.2: continued.

#	Name (km)	\mathcal{D} (km)	$\delta\mathcal{D}$	Method	Reference
200	Dynamene	133.8	5.2	STM	Usui et al. (2011)
200	Dynamene	130.5	8.6	NEATM	Masiero et al. (2011)
200	Dynamene	121.5	111.6	NEATM	Nugent et al. (2015)
200	Dynamene	120.1	123.3	NEATM	Nugent et al. (2015)
205	Martha	80.6	4.2	STM	Tedesco et al. (2004b)
205	Martha	78.0	15.0	STM	Tedesco et al. (2004a)
205	Martha	82.2	3.2	NEATM	Usui et al. (2011)
205	Martha	68.5	5.6	STM	Ryan & Woodward (2010)
205	Martha	79.8	10.8	NEATM	Ryan & Woodward (2010)
205	Martha	65.5	1.6	STM	Ryan & Woodward (2010)
205	Martha	96.3	26.1	NEATM	Ryan & Woodward (2010)
205	Martha	81.5	2.3	NEATM	Masiero et al. (2011)
205	Martha	93.2	2.2	NEATM	Masiero et al. (2012)
205	Martha	71.4	59.3	NEATM	Nugent et al. (2015)
205	Martha	64.4	11.7	occ	Dunham et al. (2017)
205	Martha	65.7	1.2	occ	Dunham et al. (2017)
211	Isolda	166.0	49.8	STM	Morrison & Zellner (2007)
211	Isolda	143.2	15.3	STM	Tedesco et al. (2004b)
211	Isolda	142.6	13.1	STM	Ryan & Woodward (2010)
211	Isolda	150.9	22.5	NEATM	Ryan & Woodward (2010)
211	Isolda	153.5	5.1	STM	Usui et al. (2011)
211	Isolda	143.0	64.9	NEATM	Masiero et al. (2011)
211	Isolda	154.2	51.3	NEATM	Masiero et al. (2012)
211	Isolda	142.5	144.2	NEATM	Nugent et al. (2015)
238	Hypatia	154.0	46.2	STM	Morrison & Zellner (2007)
238	Hypatia	145.9	23.0	occ	Dunham et al. (2017)
238	Hypatia	148.5	10.8	STM	Tedesco et al. (2004b)
238	Hypatia	149.2	42.5	STM	Ryan & Woodward (2010)
238	Hypatia	163.6	21.5	NEATM	Ryan & Woodward (2010)
238	Hypatia	144.0	4.6	STM	Usui et al. (2011)
238	Hypatia	146.5	26.0	NEATM	Masiero et al. (2011)
238	Hypatia	135.6	4.5	NEATM	Masiero et al. (2012)
238	Hypatia	176.7	154.5	NEATM	Nugent et al. (2015)
266	Aline	125.8	19.5	STM	Tedesco et al. (2004a)
266	Aline	109.1	8.7	STM	Tedesco et al. (2004b)
266	Aline	112.9	8.3	STM	Ryan & Woodward (2010)
266	Aline	125.2	25.2	NEATM	Ryan & Woodward (2010)
266	Aline	102.0	4.2	STM	Usui et al. (2011)
266	Aline	109.0	55.0	NEATM	Masiero et al. (2011)
266	Aline	152.5	190.2	NEATM	Masiero et al. (2012)
266	Aline	89.4	79.0	NEATM	Nugent et al. (2015)
303	Josephina	99.3	5.7	STM	Tedesco et al. (2004b)
303	Josephina	98.7	5.2	NEATM	Usui et al. (2011)
303	Josephina	105.4	1.6	NEATM	Hasegawa et al. (2013)
303	Josephina	100.5	8.9	STM	Ryan & Woodward (2010)
303	Josephina	105.6	20.3	NEATM	Ryan & Woodward (2010)
303	Josephina	105.9	9.3	NEATM	Masiero et al. (2011)
303	Josephina	124.9	2.8	NEATM	Masiero et al. (2012)
303	Josephina	97.6	0.8	occ	Dunham et al. (2017)
345	Tercidina	94.1	14.7	STM	Tedesco et al. (2004b)
345	Tercidina	99.3	4.2	occ	Dunham et al. (2017)
345	Tercidina	93.8	17.7	STM	Ryan & Woodward (2010)
345	Tercidina	106.2	23.4	NEATM	Ryan & Woodward (2010)
345	Tercidina	99.2	3.0	STM	Usui et al. (2011)
345	Tercidina	99.0	34.4	NEATM	Masiero et al. (2011)
345	Tercidina	101.8	79.3	NEATM	Masiero et al. (2012)
345	Tercidina	96.0	30.0	LCOCC	Hanuš et al. (2013a)
350	Ornamenta	118.3	13.5	STM	Tedesco et al. (2004b)
350	Ornamenta	117.2	4.5	NEATM	Usui et al. (2011)
350	Ornamenta	109.8	12.3	STM	Ryan & Woodward (2010)

Table D.2: continued.

#	Name (km)	\mathcal{D} (km)	$\delta\mathcal{D}$	Method	Reference
350	Ornamenta	126.3	18.4	NEATM	Ryan & Woodward (2010)
350	Ornamenta	99.5	19.1	NEATM	Masiero et al. (2011)
350	Ornamenta	99.5	32.0	NEATM	Masiero et al. (2011)
350	Ornamenta	101.6	108.0	NEATM	Nugent et al. (2015)
350	Ornamenta	99.4	7.3	OCC	Dunham et al. (2017)
356	Liguria	155.0	46.5	STM	Morrison & Zellner (2007)
356	Liguria	126.6	31.8	OCC	Dunham et al. (2017)
356	Liguria	131.3	7.8	STM	Tedesco et al. (2004b)
356	Liguria	135.7	15.2	STM	Ryan & Woodward (2010)
356	Liguria	135.1	21.2	NEATM	Ryan & Woodward (2010)
356	Liguria	136.6	5.6	STM	Usui et al. (2011)
356	Liguria	131.0	29.1	NEATM	Masiero et al. (2011)
356	Liguria	145.5	4.3	NEATM	Masiero et al. (2012)
358	Apollonia	89.4	8.1	STM	Tedesco et al. (2004b)
358	Apollonia	89.4	3.7	NEATM	Usui et al. (2011)
358	Apollonia	83.7	10.1	STM	Ryan & Woodward (2010)
358	Apollonia	88.1	12.0	NEATM	Ryan & Woodward (2010)
358	Apollonia	90.5	6.4	NEATM	Masiero et al. (2011)
358	Apollonia	93.4	77.8	NEATM	Nugent et al. (2015)
358	Apollonia	87.8	81.8	NEATM	Nugent et al. (2015)
362	Havnia	85.1	3.1	NEATM	Usui et al. (2011)
362	Havnia	89.2	6.4	NEATM	Masiero et al. (2011)
362	Havnia	92.0	2.6	NEATM	Masiero et al. (2012)
366	Vincentina	93.8	9.6	STM	Tedesco et al. (2004b)
366	Vincentina	86.2	2.2	NEATM	Usui et al. (2011)
366	Vincentina	93.6	15.2	STM	Ryan & Woodward (2010)
366	Vincentina	98.2	13.9	NEATM	Ryan & Woodward (2010)
366	Vincentina	94.4	6.2	NEATM	Masiero et al. (2011)
366	Vincentina	89.5	88.4	NEATM	Nugent et al. (2015)
366	Vincentina	85.0	39.6	OCC	Dunham et al. (2017)
366	Vincentina	82.0	89.7	OCC	Dunham et al. (2017)
373	Melusina	95.8	11.1	STM	Tedesco et al. (2004b)
373	Melusina	96.7	3.7	NEATM	Usui et al. (2011)
373	Melusina	84.9	9.4	STM	Ryan & Woodward (2010)
373	Melusina	107.7	17.4	NEATM	Ryan & Woodward (2010)
373	Melusina	91.6	4.8	NEATM	Masiero et al. (2011)
373	Melusina	98.7	2.8	NEATM	Masiero et al. (2012)
373	Melusina	90.4	88.8	NEATM	Nugent et al. (2015)
377	Campania	91.1	6.0	STM	Tedesco et al. (2004b)
377	Campania	92.6	3.3	NEATM	Usui et al. (2011)
377	Campania	75.3	7.0	STM	Ryan & Woodward (2010)
377	Campania	96.4	16.9	NEATM	Ryan & Woodward (2010)
377	Campania	94.0	20.1	NEATM	Masiero et al. (2011)
377	Campania	91.0	224.7	OCC	Dunham et al. (2017)
404	Arsinoe	101.0	30.3	STM	Morrison & Zellner (2007)
404	Arsinoe	97.7	4.5	STM	Tedesco et al. (2004b)
404	Arsinoe	98.8	9.6	OCC	Dunham et al. (2017)
404	Arsinoe	98.4	12.5	STM	Ryan & Woodward (2010)
404	Arsinoe	102.3	13.6	NEATM	Ryan & Woodward (2010)
404	Arsinoe	93.0	3.4	STM	Usui et al. (2011)
404	Arsinoe	98.7	10.4	NEATM	Masiero et al. (2011)
404	Arsinoe	108.6	3.3	NEATM	Masiero et al. (2012)
404	Arsinoe	101.0	15.0	LCOCC	Hanuš et al. (2013a)
404	Arsinoe	85.1	84.8	NEATM	Nugent et al. (2015)
405	Thia	124.9	6.9	STM	Tedesco et al. (2004b)
405	Thia	129.6	11.9	STM	Ryan & Woodward (2010)
405	Thia	134.9	20.2	NEATM	Ryan & Woodward (2010)
405	Thia	113.3	5.2	STM	Usui et al. (2011)
405	Thia	125.0	52.3	NEATM	Masiero et al. (2011)
405	Thia	101.5	100.6	NEATM	Nugent et al. (2015)

Table D.2: continued.

#	Name (km)	\mathcal{D} (km)	$\delta\mathcal{D}$	Method	Reference
407	Arachne	95.1	16.2	STM	Tedesco et al. (2004b)
407	Arachne	97.5	4.8	NEATM	Usui et al. (2011)
407	Arachne	82.2	8.9	STM	Ryan & Woodward (2010)
407	Arachne	97.8	14.8	NEATM	Ryan & Woodward (2010)
407	Arachne	86.3	62.7	NEATM	Nugent et al. (2015)
410	Chloris	135.0	40.5	STM	Morrison & Zellner (2007)
410	Chloris	123.6	16.2	STM	Tedesco et al. (2004b)
410	Chloris	118.0	15.7	STM	Ryan & Woodward (2010)
410	Chloris	124.2	16.5	NEATM	Ryan & Woodward (2010)
410	Chloris	106.7	4.3	STM	Usui et al. (2011)
410	Chloris	118.9	8.6	NEATM	Masiero et al. (2011)
410	Chloris	96.8	87.5	NEATM	Nugent et al. (2015)
442	Eichsfeldia	66.7	4.2	STM	Tedesco et al. (2004b)
442	Eichsfeldia	68.7	5.9	STM	Ryan & Woodward (2010)
442	Eichsfeldia	65.9	7.7	NEATM	Ryan & Woodward (2010)
442	Eichsfeldia	65.1	2.5	STM	Usui et al. (2011)
442	Eichsfeldia	63.2	3.7	NEATM	Masiero et al. (2011)
442	Eichsfeldia	61.6	60.5	NEATM	Nugent et al. (2015)
445	Edna	89.3	13.6	STM	Tedesco et al. (2004a)
445	Edna	87.2	6.3	STM	Tedesco et al. (2004b)
445	Edna	81.4	13.0	STM	Ryan & Woodward (2010)
445	Edna	98.2	15.9	NEATM	Ryan & Woodward (2010)
445	Edna	89.2	4.3	STM	Usui et al. (2011)
445	Edna	105.5	4.5	NEATM	Masiero et al. (2011)
445	Edna	90.2	92.6	NEATM	Nugent et al. (2015)
445	Edna	82.5	79.1	NEATM	Nugent et al. (2015)
481	Emita	113.2	9.2	STM	Tedesco et al. (2004b)
481	Emita	113.2	9.2	STM	Tedesco et al. (2004a)
481	Emita	102.0	0.0	STM	Ryan & Woodward (2010)
481	Emita	108.4	0.0	NEATM	Ryan & Woodward (2010)
481	Emita	103.5	5.7	STM	Usui et al. (2011)
481	Emita	121.6	117.9	NEATM	Masiero et al. (2012)
481	Emita	104.1	119.1	NEATM	Nugent et al. (2015)
488	Kreusa	150.1	19.2	STM	Tedesco et al. (2004b)
488	Kreusa	156.0	20.8	STM	Ryan & Woodward (2010)
488	Kreusa	161.6	22.2	NEATM	Ryan & Woodward (2010)
488	Kreusa	172.6	7.6	STM	Usui et al. (2011)
488	Kreusa	150.0	34.0	NEATM	Masiero et al. (2011)
488	Kreusa	168.1	6.2	NEATM	Masiero et al. (2012)
488	Kreusa	143.9	156.2	NEATM	Nugent et al. (2015)
488	Kreusa	161.5	145.5	NEATM	Nugent et al. (2015)
490	Veritas	108.1	13.8	OCC	Dunham et al. (2017)
490	Veritas	115.6	16.5	STM	Tedesco et al. (2004b)
490	Veritas	131.5	12.0	IM	Marchis et al. (2006)
490	Veritas	102.9	15.8	STM	Ryan & Woodward (2010)
490	Veritas	112.0	15.2	NEATM	Ryan & Woodward (2010)
490	Veritas	112.8	5.0	STM	Usui et al. (2011)
490	Veritas	118.8	5.5	NEATM	Masiero et al. (2012)
490	Veritas	100.8	88.9	NEATM	Nugent et al. (2015)
490	Veritas	108.4	108.0	NEATM	Nugent et al. (2015)
503	Evelyn	81.7	14.7	STM	Tedesco et al. (2004b)
503	Evelyn	83.4	14.7	STM	Ryan & Woodward (2010)
503	Evelyn	83.6	29.7	NEATM	Ryan & Woodward (2010)
503	Evelyn	90.2	3.1	STM	Usui et al. (2011)
503	Evelyn	99.2	102.8	NEATM	Masiero et al. (2012)
521	Brixia	115.7	6.0	STM	Tedesco et al. (2004b)
521	Brixia	109.3	15.6	OCC	Dunham et al. (2017)
521	Brixia	125.4	4.9	NEATM	Usui et al. (2011)
521	Brixia	108.2	12.6	STM	Ryan & Woodward (2010)
521	Brixia	120.0	15.9	NEATM	Ryan & Woodward (2010)

Table D.2: continued.

#	Name (km)	\mathcal{D} (km)	$\delta\mathcal{D}$	Method	Reference
521	Brixia	111.9	12.2	NEATM	Masiero et al. (2011)
521	Brixia	110.6	8.9	NEATM	Masiero et al. (2011)
521	Brixia	104.6	91.8	NEATM	Nugent et al. (2015)
521	Brixia	104.0	110.9	NEATM	Nugent et al. (2015)
554	Peraga	101.0	30.3	STM	Morrison & Zellner (2007)
554	Peraga	95.9	12.3	STM	Tedesco et al. (2004b)
554	Peraga	93.9	10.2	STM	Ryan & Woodward (2010)
554	Peraga	109.1	17.0	NEATM	Ryan & Woodward (2010)
554	Peraga	97.0	3.5	STM	Usui et al. (2011)
554	Peraga	102.8	81.8	NEATM	Masiero et al. (2012)
554	Peraga	89.4	91.0	NEATM	Nugent et al. (2015)
602	Marianna	137.0	41.1	STM	Morrison & Zellner (2007)
602	Marianna	124.7	6.6	STM	Tedesco et al. (2004b)
602	Marianna	111.1	10.5	STM	Ryan & Woodward (2010)
602	Marianna	130.1	16.6	NEATM	Ryan & Woodward (2010)
602	Marianna	129.9	5.8	STM	Usui et al. (2011)
602	Marianna	126.8	6.2	NEATM	Masiero et al. (2011)
654	Zelinda	127.4	11.7	STM	Tedesco et al. (2004b)
654	Zelinda	129.1	11.4	STM	Tedesco et al. (2004a)
654	Zelinda	119.3	52.6	OCC	Dunham et al. (2017)
654	Zelinda	112.5	12.0	IM	Marchis et al. (2006)
654	Zelinda	138.0	13.9	STM	Ryan & Woodward (2010)
654	Zelinda	134.3	18.8	NEATM	Ryan & Woodward (2010)
654	Zelinda	123.6	4.4	STM	Usui et al. (2011)
654	Zelinda	127.0	61.4	NEATM	Masiero et al. (2011)
654	Zelinda	160.7	4.0	NEATM	Masiero et al. (2012)
654	Zelinda	135.9	119.1	NEATM	Nugent et al. (2015)
654	Zelinda	134.8	116.8	NEATM	Nugent et al. (2015)
694	Ekard	101.0	30.3	STM	Morrison & Zellner (2007)
694	Ekard	90.8	12.0	STM	Tedesco et al. (2004b)
694	Ekard	99.2	21.8	STM	Tedesco et al. (2004a)
694	Ekard	104.8	8.5	OCC	Dunham et al. (2017)
694	Ekard	95.9	110.5	OCC	Dunham et al. (2017)
694	Ekard	90.5	13.0	STM	Ryan & Woodward (2010)
694	Ekard	101.9	51.4	NEATM	Ryan & Woodward (2010)
694	Ekard	63.9	10.9	STM	Ryan & Woodward (2010)
694	Ekard	92.8	17.0	NEATM	Ryan & Woodward (2010)
694	Ekard	92.1	3.8	STM	Usui et al. (2011)
694	Ekard	121.9	2.2	STM	Masiero et al. (2012)
694	Ekard	98.9	76.2	NEATM	Nugent et al. (2015)
735	Marghanna	74.3	4.8	STM	Tedesco et al. (2004b)
735	Marghanna	65.1	5.9	STM	Ryan & Woodward (2010)
735	Marghanna	76.9	11.2	NEATM	Ryan & Woodward (2010)
735	Marghanna	78.7	4.9	STM	Usui et al. (2011)
735	Marghanna	70.6	3.7	NEATM	Masiero et al. (2011)
735	Marghanna	70.8	3.8	NEATM	Masiero et al. (2011)
735	Marghanna	57.2	78.2	NEATM	Nugent et al. (2015)
751	Faina	110.5	12.9	STM	Tedesco et al. (2004b)
751	Faina	109.6	23.7	STM	Ryan & Woodward (2010)
751	Faina	122.5	18.7	NEATM	Ryan & Woodward (2010)
751	Faina	106.8	3.8	STM	Usui et al. (2011)
751	Faina	106.3	4.9	NEATM	Masiero et al. (2011)
751	Faina	123.7	130.4	NEATM	Nugent et al. (2015)
776	Berbericia	151.2	12.0	STM	Tedesco et al. (2004b)
776	Berbericia	172.4	80.4	OCC	Dunham et al. (2017)
776	Berbericia	155.8	15.4	STM	Ryan & Woodward (2010)
776	Berbericia	165.9	31.1	NEATM	Ryan & Woodward (2010)
776	Berbericia	149.8	5.3	STM	Usui et al. (2011)
776	Berbericia	151.1	12.3	NEATM	Masiero et al. (2011)
776	Berbericia	135.1	102.9	NEATM	Nugent et al. (2015)

Table D.2: continued.

#	Name (km)	\mathcal{D} (km)	$\delta\mathcal{D}$	Method	Reference
788	Hohensteina	103.7	10.2	STM	Tedesco et al. (2004b)
788	Hohensteina	105.5	13.5	occ	Dunham et al. (2017)
788	Hohensteina	100.6	7.5	occ	Dunham et al. (2017)
788	Hohensteina	118.3	5.0	NEATM	Usui et al. (2011)
788	Hohensteina	108.1	11.2	STM	Ryan & Woodward (2010)
788	Hohensteina	121.0	23.3	NEATM	Ryan & Woodward (2010)
788	Hohensteina	118.3	8.2	NEATM	Masiero et al. (2011)
788	Hohensteina	125.8	4.5	NEATM	Masiero et al. (2012)
788	Hohensteina	101.2	97.4	NEATM	Nugent et al. (2015)
791	Ani	103.5	5.7	STM	Tedesco et al. (2004b)
791	Ani	82.5	9.6	occ	Dunham et al. (2017)
791	Ani	85.9	26.9	occ	Dunham et al. (2017)
791	Ani	97.9	3.4	NEATM	Usui et al. (2011)
791	Ani	93.4	8.5	STM	Ryan & Woodward (2010)
791	Ani	115.0	14.0	NEATM	Ryan & Woodward (2010)
791	Ani	82.5	17.9	NEATM	Masiero et al. (2011)
791	Ani	116.9	3.1	NEATM	Masiero et al. (2012)
791	Ani	83.3	63.9	NEATM	Nugent et al. (2015)
914	Palisana	80.5	5.8	STM	Tedesco et al. (2004a)
914	Palisana	76.6	5.1	STM	Tedesco et al. (2004b)
914	Palisana	91.2	7.8	occ	Dunham et al. (2017)
914	Palisana	76.5	15.0	IM	Marchis et al. (2006)
914	Palisana	67.0	6.3	STM	Ryan & Woodward (2010)
914	Palisana	83.6	11.3	NEATM	Ryan & Woodward (2010)
914	Palisana	97.3	4.5	STM	Usui et al. (2011)
914	Palisana	77.0	39.4	NEATM	Masiero et al. (2011)
914	Palisana	78.9	61.3	NEATM	Nugent et al. (2015)
1467	Mashona	95.1	3.9	NEATM	Usui et al. (2011)

Table D.3: The mass (\mathcal{M}) for all the Ch/Cgh asteroids available in the literature. For each, the 3σ uncertainty, method, and bibliographic reference are reported. The methods are **DEFL**: Deflection, **EPHEM**: Ephemeris, **BIMG**: Binary: Imaging, and **BGENO**: Binary: Genoid.

#	Name	\mathcal{M} (kg)	$\delta\mathcal{M}$	Method	Reference
13	Egeria	1.63×10^{19}	9.54×10^{18}	DEFL	Baer et al. (2008)
13	Egeria	6.17×10^{18}	1.85×10^{18}	EPHEM	Folkner et al. (2009)
13	Egeria	1.59×10^{19}	1.31×10^{19}	DEFL	Baer et al. (2011)
13	Egeria	1.29×10^{19}	1.41×10^{19}	DEFL	Zielenbach (2011)
13	Egeria	7.39×10^{18}	9.72×10^{18}	DEFL	Zielenbach (2011)
13	Egeria	6.07×10^{18}	9.60×10^{18}	DEFL	Zielenbach (2011)
13	Egeria	8.26×10^{18}	1.83×10^{19}	DEFL	Zielenbach (2011)
13	Egeria	9.37×10^{18}	4.65×10^{18}	EPHEM	Fienga et al. (2013)
13	Egeria	1.23×10^{19}	9.90×10^{18}	EPHEM	Kuchynka & Folkner (2013)
13	Egeria	9.37×10^{18}	7.08×10^{18}	EPHEM	Fienga et al. (2014)
13	Egeria	9.35×10^{18}	2.39×10^{18}	DEFL	Goffin (2014)
13	Egeria	9.62×10^{18}	4.47×10^{18}	DEFL	Kochetova & Chernetenko (2014)
13	Egeria	1.04×10^{19}	4.65×10^{18}	EPHEM	Viswanathan et al. (2017)
13	Egeria	2.25×10^{19}	7.83×10^{19}	DEFL	Siltala & Granvik (2017)
13	Egeria	1.08×10^{19}	4.38×10^{18}	EPHEM	Fienga (2018)
19	Fortuna	1.27×10^{19}	1.49×10^{18}	DEFL	Baer et al. (2008)
19	Fortuna	4.02×10^{18}	1.19×10^{18}	EPHEM	Fienga et al. (2009)
19	Fortuna	6.94×10^{18}	2.08×10^{18}	EPHEM	Folkner et al. (2009)
19	Fortuna	6.37×10^{18}	8.70×10^{18}	DEFL	Somenzi et al. (2010)
19	Fortuna	8.31×10^{18}	2.15×10^{18}	DEFL	Baer et al. (2011)
19	Fortuna	6.37×10^{18}	3.15×10^{18}	EPHEM	Konopliv et al. (2011)
19	Fortuna	1.00×10^{19}	3.24×10^{18}	DEFL	Zielenbach (2011)
19	Fortuna	1.02×10^{19}	2.84×10^{18}	DEFL	Zielenbach (2011)
19	Fortuna	1.01×10^{19}	2.81×10^{18}	DEFL	Zielenbach (2011)
19	Fortuna	1.05×10^{19}	3.69×10^{18}	DEFL	Zielenbach (2011)
19	Fortuna	8.35×10^{18}	1.79×10^{18}	EPHEM	Fienga et al. (2011)
19	Fortuna	9.73×10^{18}	3.03×10^{18}	EPHEM	Fienga et al. (2013)
19	Fortuna	7.79×10^{18}	2.70×10^{18}	EPHEM	Kuchynka & Folkner (2013)
19	Fortuna	8.67×10^{18}	7.77×10^{17}	EPHEM	Pitjeva (2013)
19	Fortuna	8.00×10^{18}	2.81×10^{18}	EPHEM	Fienga et al. (2014)
19	Fortuna	8.95×10^{18}	5.97×10^{17}	DEFL	Goffin (2014)
19	Fortuna	8.83×10^{18}	1.25×10^{18}	DEFL	Kochetova & Chernetenko (2014)
19	Fortuna	1.03×10^{19}	1.68×10^{18}	EPHEM	Viswanathan et al. (2017)
19	Fortuna	2.80×10^{18}	9.33×10^{18}	DEFL	Siltala & Granvik (2017)
19	Fortuna	2.21×10^{19}	3.03×10^{19}	DEFL	Siltala & Granvik (2017)
19	Fortuna	1.10×10^{19}	1.90×10^{18}	EPHEM	Baer & Chesley (2017)
19	Fortuna	1.17×10^{19}	1.42×10^{18}	EPHEM	Fienga (2018)
34	Circe	3.68×10^{18}	4.53×10^{18}	EPHEM	Fienga et al. (2011)
34	Circe	2.89×10^{18}	3.63×10^{18}	EPHEM	Fienga et al. (2013)
34	Circe	4.18×10^{18}	1.19×10^{18}	DEFL	Goffin (2014)
34	Circe	5.01×10^{18}	4.86×10^{18}	EPHEM	Viswanathan et al. (2017)
34	Circe	5.96×10^{18}	5.19×10^{18}	EPHEM	Fienga (2018)
38	Leda	3.18×10^{18}	1.79×10^{18}	DEFL	Goffin (2014)
38	Leda	6.03×10^{18}	4.38×10^{18}	EPHEM	Viswanathan et al. (2017)
38	Leda	7.07×10^{18}	4.44×10^{18}	EPHEM	Fienga (2018)
41	Daphne	1.05×10^{19}	2.99×10^{18}	EPHEM	Fienga et al. (2009)
41	Daphne	7.90×10^{18}	2.37×10^{18}	EPHEM	Folkner et al. (2009)
41	Daphne	8.43×10^{18}	1.06×10^{19}	EPHEM	Konopliv et al. (2011)
41	Daphne	1.82×10^{19}	2.16×10^{19}	DEFL	Zielenbach (2011)
41	Daphne	3.02×10^{17}	1.70×10^{19}	DEFL	Zielenbach (2011)
41	Daphne	4.76×10^{18}	1.65×10^{19}	DEFL	Zielenbach (2011)
41	Daphne	1.21×10^{19}	3.15×10^{19}	DEFL	Zielenbach (2011)
41	Daphne	1.02×10^{19}	3.57×10^{18}	EPHEM	Fienga et al. (2011)
41	Daphne	7.79×10^{18}	5.40×10^{18}	EPHEM	Kuchynka & Folkner (2013)

Table D.3: continued.

#	Name (kg)	M (kg)	δM	Method	Reference
41	Daphne	8.29×10^{18}	2.62×10^{18}	EPHEM	Pitjeva (2013)
41	Daphne	7.13×10^{18}	2.01×10^{18}	EPHEM	Fienga et al. (2014)
41	Daphne	9.35×10^{18}	4.17×10^{18}	DEFL	Goffin (2014)
41	Daphne	9.78×10^{18}	1.38×10^{19}	DEFL	Kochetova & Chernetenko (2014)
41	Daphne	4.44×10^{18}	2.52×10^{18}	EPHEM	Fienga (2018)
41	Daphne	5.95×10^{18}	1.70×10^{18}	BGENO	This work
48	Doris	1.21×10^{19}	1.79×10^{19}	DEFL	Kochetova (2004)
48	Doris	5.89×10^{18}	1.45×10^{19}	DEFL	Zielenbach (2011)
48	Doris	3.78×10^{18}	1.12×10^{19}	DEFL	Zielenbach (2011)
48	Doris	3.84×10^{18}	1.11×10^{19}	DEFL	Zielenbach (2011)
48	Doris	7.94×10^{18}	1.92×10^{19}	DEFL	Zielenbach (2011)
48	Doris	2.40×10^{19}	2.05×10^{19}	EPHEM	Fienga et al. (2011)
48	Doris	5.99×10^{15}	1.13×10^{17}	EPHEM	Fienga et al. (2014)
48	Doris	7.76×10^{18}	1.79×10^{18}	DEFL	Goffin (2014)
48	Doris	1.75×10^{19}	1.54×10^{19}	EPHEM	Fienga (2018)
49	Pales	2.69×10^{18}	1.49×10^{18}	DEFL	Baer et al. (2008)
49	Pales	5.07×10^{18}	1.16×10^{19}	DEFL	Zielenbach (2011)
49	Pales	8.11×10^{18}	8.04×10^{18}	DEFL	Zielenbach (2011)
49	Pales	7.61×10^{18}	8.01×10^{18}	DEFL	Zielenbach (2011)
49	Pales	4.93×10^{18}	1.47×10^{19}	DEFL	Zielenbach (2011)
49	Pales	5.37×10^{18}	1.79×10^{18}	DEFL	Goffin (2014)
49	Pales	7.59×10^{18}	5.52×10^{18}	EPHEM	Fienga (2018)
50	Virginia	1.95×10^{18}	2.18×10^{18}	EPHEM	Fienga et al. (2011)
50	Virginia	5.97×10^{17}	1.79×10^{17}	DEFL	Goffin (2014)
50	Virginia	1.46×10^{18}	1.16×10^{18}	EPHEM	Fienga (2018)
51	Nemausa	2.16×10^{18}	6.48×10^{17}	EPHEM	Folkner et al. (2009)
51	Nemausa	4.55×10^{18}	8.16×10^{18}	DEFL	Zielenbach (2011)
51	Nemausa	3.39×10^{18}	4.86×10^{18}	DEFL	Zielenbach (2011)
51	Nemausa	3.36×10^{18}	4.86×10^{18}	DEFL	Zielenbach (2011)
51	Nemausa	4.25×10^{18}	6.24×10^{18}	DEFL	Zielenbach (2011)
51	Nemausa	5.63×10^{18}	3.90×10^{18}	EPHEM	Fienga et al. (2011)
51	Nemausa	1.79×10^{16}	2.69×10^{16}	EPHEM	Fienga et al. (2013)
51	Nemausa	4.76×10^{15}	1.65×10^{18}	EPHEM	Fienga et al. (2014)
51	Nemausa	2.78×10^{18}	1.19×10^{18}	DEFL	Goffin (2014)
51	Nemausa	4.79×10^{18}	2.53×10^{18}	EPHEM	Baer & Chesley (2017)
51	Nemausa	4.22×10^{18}	2.26×10^{18}	EPHEM	Baer & Chesley (2017)
51	Nemausa	3.98×10^{18}	2.54×10^{18}	EPHEM	Fienga (2018)
54	Alexandra	1.08×10^{19}	1.83×10^{19}	DEFL	Zielenbach (2011)
54	Alexandra	1.74×10^{18}	9.57×10^{18}	DEFL	Zielenbach (2011)
54	Alexandra	2.94×10^{18}	9.45×10^{18}	DEFL	Zielenbach (2011)
54	Alexandra	6.44×10^{18}	2.08×10^{19}	DEFL	Zielenbach (2011)
54	Alexandra	1.03×10^{19}	5.22×10^{18}	EPHEM	Fienga et al. (2011)
54	Alexandra	1.67×10^{19}	6.45×10^{18}	EPHEM	Fienga et al. (2013)
54	Alexandra	1.21×10^{19}	3.42×10^{18}	EPHEM	Viswanathan et al. (2017)
54	Alexandra	1.62×10^{18}	2.02×10^{18}	EPHEM	Fienga (2018)
58	Concordia	1.28×10^{17}	1.92×10^{17}	EPHEM	Fienga (2018)
62	Erato	1.38×10^{17}	2.07×10^{17}	EPHEM	Fienga (2018)
70	Panopaea	4.33×10^{18}	3.27×10^{18}	EPHEM	Fienga et al. (2011)
70	Panopaea	3.38×10^{18}	1.19×10^{18}	DEFL	Goffin (2014)
70	Panopaea	4.67×10^{18}	2.95×10^{18}	EPHEM	Fienga (2018)
78	Diana	1.27×10^{18}	3.81×10^{17}	EPHEM	Folkner et al. (2009)
78	Diana	5.09×10^{18}	3.39×10^{18}	EPHEM	Fienga et al. (2013)
78	Diana	4.29×10^{17}	8.07×10^{17}	EPHEM	Viswanathan et al. (2017)
78	Diana	3.76×10^{17}	5.34×10^{17}	EPHEM	Fienga (2018)
84	Klio	5.45×10^{17}	8.04×10^{17}	EPHEM	Viswanathan et al. (2017)
84	Klio	7.60×10^{17}	7.32×10^{17}	EPHEM	Fienga (2018)

Table D.3: continued.

#	Name (kg)	M (kg)	δM	Method	Reference
91	Aegina	6.07×10^{17}	8.94×10^{17}	EPHEM	Viswanathan et al. (2017)
91	Aegina	2.00×10^{17}	2.99×10^{17}	EPHEM	Fienga (2018)
95	Arethusa	4.18×10^{18}	2.39×10^{18}	DEFL	Goffin (2014)
95	Arethusa	6.86×10^{18}	8.91×10^{18}	EPHEM	Viswanathan et al. (2017)
95	Arethusa	7.46×10^{18}	9.30×10^{18}	EPHEM	Fienga (2018)
98	Ianthe	8.24×10^{17}	2.47×10^{17}	EPHEM	Folkner et al. (2009)
98	Ianthe	1.47×10^{18}	2.07×10^{18}	EPHEM	Fienga et al. (2011)
98	Ianthe	1.65×10^{18}	2.23×10^{18}	EPHEM	Viswanathan et al. (2017)
98	Ianthe	1.55×10^{18}	2.02×10^{18}	EPHEM	Fienga (2018)
104	Klymene	1.79×10^{18}	1.19×10^{18}	DEFL	Goffin (2014)
104	Klymene	3.78×10^{18}	4.80×10^{18}	EPHEM	Fienga (2018)
105	Artemis	1.32×10^{18}	3.96×10^{17}	EPHEM	Folkner et al. (2009)
105	Artemis	2.89×10^{18}	2.53×10^{18}	EPHEM	Fienga et al. (2011)
105	Artemis	6.06×10^{18}	3.81×10^{18}	EPHEM	Fienga et al. (2013)
105	Artemis	2.63×10^{18}	1.82×10^{18}	EPHEM	Viswanathan et al. (2017)
105	Artemis	1.91×10^{18}	1.82×10^{18}	EPHEM	Fienga (2018)
106	Dione	3.04×10^{17}	1.08×10^{19}	DEFL	Zielenbach (2011)
106	Dione	4.29×10^{18}	7.92×10^{18}	DEFL	Zielenbach (2011)
106	Dione	3.52×10^{18}	7.86×10^{18}	DEFL	Zielenbach (2011)
106	Dione	3.77×10^{18}	1.74×10^{19}	DEFL	Zielenbach (2011)
106	Dione	7.70×10^{18}	2.44×10^{18}	EPHEM	Fienga et al. (2013)
106	Dione	3.58×10^{18}	1.79×10^{18}	DEFL	Goffin (2014)
106	Dione	1.08×10^{17}	1.62×10^{17}	EPHEM	Fienga (2018)
109	Felicitas	3.20×10^{17}	1.49×10^{18}	EPHEM	Fienga et al. (2013)
109	Felicitas	2.21×10^{18}	1.55×10^{18}	EPHEM	Fienga et al. (2014)
109	Felicitas	1.65×10^{17}	2.44×10^{17}	EPHEM	Fienga (2018)
111	Ate	1.99×10^{18}	5.97×10^{17}	DEFL	Krasinsky et al. (2001)
111	Ate	1.67×10^{20}	1.13×10^{20}	DEFL	Ivantsov (2008)
111	Ate	1.74×10^{18}	5.22×10^{17}	EPHEM	Folkner et al. (2009)
111	Ate	2.71×10^{18}	7.47×10^{18}	DEFL	Zielenbach (2011)
111	Ate	3.42×10^{17}	4.95×10^{18}	DEFL	Zielenbach (2011)
111	Ate	8.16×10^{17}	4.98×10^{18}	DEFL	Zielenbach (2011)
111	Ate	8.93×10^{18}	7.05×10^{18}	EPHEM	Fienga et al. (2013)
111	Ate	5.87×10^{17}	5.94×10^{18}	EPHEM	Fienga et al. (2014)
111	Ate	3.05×10^{18}	3.45×10^{18}	EPHEM	Viswanathan et al. (2017)
111	Ate	3.60×10^{18}	3.15×10^{18}	EPHEM	Fienga (2018)
112	Iphigenia	4.52×10^{17}	6.36×10^{17}	EPHEM	Fienga (2018)
121	Hermione	9.35×10^{18}	4.77×10^{18}	DEFL	Viateau (2000)
121	Hermione	5.38×10^{18}	8.94×10^{17}	BIMG	Marchis et al. (2005)
121	Hermione	4.70×10^{18}	6.00×10^{17}	BIMG	Descamps et al. (2009)
121	Hermione	5.12×10^{18}	6.66×10^{18}	DEFL	Zielenbach (2011)
121	Hermione	6.01×10^{18}	5.10×10^{18}	DEFL	Zielenbach (2011)
121	Hermione	4.58×10^{18}	6.39×10^{18}	DEFL	Zielenbach (2011)
121	Hermione	6.27×10^{18}	6.84×10^{18}	DEFL	Zielenbach (2011)
121	Hermione	3.18×10^{18}	1.19×10^{18}	DEFL	Goffin (2014)
121	Hermione	4.77×10^{18}	2.39×10^{18}	DEFL	Kretlow (2014)
121	Hermione	6.69×10^{18}	7.65×10^{18}	EPHEM	Viswanathan et al. (2017)
121	Hermione	5.53×10^{18}	3.13×10^{18}	EPHEM	Baer & Chesley (2017)
121	Hermione	7.29×10^{18}	7.44×10^{18}	EPHEM	Fienga (2018)
127	Johanna	3.08×10^{18}	4.05×10^{18}	EPHEM	Fienga et al. (2011)
127	Johanna	1.67×10^{18}	4.14×10^{18}	EPHEM	Fienga (2018)
130	Elektra	6.60×10^{18}	1.19×10^{18}	BIMG	Marchis et al. (2008b)
130	Elektra	1.61×10^{19}	2.51×10^{19}	DEFL	Zielenbach (2011)
130	Elektra	1.00×10^{19}	1.97×10^{19}	DEFL	Zielenbach (2011)
130	Elektra	6.93×10^{18}	1.93×10^{19}	DEFL	Zielenbach (2011)
130	Elektra	1.34×10^{19}	3.90×10^{19}	DEFL	Zielenbach (2011)

Table D.3: continued.

#	Name (kg)	M (kg)	δM	Method	Reference
130	Elektra	2.19×10^{17}	3.57×10^{17}	EPHEM	Fienga et al. (2011)
130	Elektra	1.39×10^{19}	4.77×10^{18}	DEFL	Goffin (2014)
130	Elektra	9.41×10^{18}	6.27×10^{18}	EPHEM	Viswanathan et al. (2017)
130	Elektra	7.46×10^{18}	6.27×10^{18}	EPHEM	Fienga (2018)
130	Elektra	6.20×10^{18}	6.00×10^{16}	BIMG	Yang et al. (2016)
134	Sophrosyne	2.02×10^{18}	2.21×10^{18}	EPHEM	Fienga et al. (2013)
134	Sophrosyne	4.92×10^{18}	3.45×10^{18}	EPHEM	Viswanathan et al. (2017)
134	Sophrosyne	5.68×10^{17}	8.34×10^{17}	EPHEM	Fienga (2018)
141	Lumen	8.31×10^{18}	2.80×10^{18}	EPHEM	Viswanathan et al. (2017)
141	Lumen	3.27×10^{18}	2.80×10^{18}	EPHEM	Fienga (2018)
144	Vibia	4.63×10^{18}	8.52×10^{18}	DEFL	Zielenbach (2011)
144	Vibia	5.32×10^{18}	5.58×10^{18}	DEFL	Zielenbach (2011)
144	Vibia	4.95×10^{18}	5.55×10^{18}	DEFL	Zielenbach (2011)
144	Vibia	4.62×10^{18}	9.18×10^{18}	DEFL	Zielenbach (2011)
144	Vibia	1.61×10^{15}	5.97×10^{15}	EPHEM	Fienga et al. (2014)
144	Vibia	3.38×10^{18}	1.19×10^{18}	DEFL	Goffin (2014)
144	Vibia	4.69×10^{18}	2.49×10^{18}	EPHEM	Fienga (2018)
145	Adeona	2.26×10^{18}	6.78×10^{17}	EPHEM	Folkner et al. (2009)
145	Adeona	1.73×10^{17}	7.17×10^{18}	DEFL	Zielenbach (2011)
145	Adeona	2.10×10^{18}	8.91×10^{18}	DEFL	Zielenbach (2011)
145	Adeona	2.04×10^{15}	6.57×10^{15}	EPHEM	Fienga et al. (2014)
145	Adeona	2.78×10^{18}	1.79×10^{18}	DEFL	Goffin (2014)
145	Adeona	3.24×10^{17}	4.80×10^{17}	EPHEM	Fienga (2018)
146	Lucina	1.18×10^{17}	1.77×10^{17}	EPHEM	Fienga (2018)
156	Xanthippe	6.49×10^{18}	2.62×10^{18}	EPHEM	Fienga et al. (2013)
156	Xanthippe	6.72×10^{17}	9.00×10^{17}	EPHEM	Fienga (2018)
159	Aemilia	4.18×10^{18}	1.79×10^{18}	DEFL	Goffin (2014)
159	Aemilia	5.72×10^{18}	7.59×10^{18}	EPHEM	Fienga (2018)
162	Laurentia	3.36×10^{17}	5.01×10^{17}	EPHEM	Fienga (2018)
163	Erigone	5.79×10^{17}	7.29×10^{17}	EPHEM	Fienga (2018)
168	Sibylla	6.02×10^{18}	2.35×10^{19}	DEFL	Zielenbach (2011)
168	Sibylla	2.38×10^{18}	1.72×10^{19}	DEFL	Zielenbach (2011)
168	Sibylla	6.33×10^{18}	7.32×10^{18}	EPHEM	Fienga (2018)
176	Iduna	3.36×10^{17}	5.04×10^{17}	EPHEM	Fienga (2018)
187	Lamberta	1.57×10^{18}	4.71×10^{17}	EPHEM	Folkner et al. (2009)
187	Lamberta	5.69×10^{18}	2.35×10^{18}	EPHEM	Fienga et al. (2014)
187	Lamberta	2.19×10^{18}	2.39×10^{18}	DEFL	Goffin (2014)
187	Lamberta	2.87×10^{17}	4.14×10^{17}	EPHEM	Viswanathan et al. (2017)
187	Lamberta	4.93×10^{17}	6.81×10^{17}	EPHEM	Fienga (2018)
195	Eurykleia	1.44×10^{17}	2.16×10^{17}	EPHEM	Fienga (2018)
200	Dynamene	1.14×10^{18}	4.17×10^{17}	EPHEM	Fienga et al. (2013)
200	Dynamene	3.98×10^{18}	1.79×10^{18}	DEFL	Goffin (2014)
205	Martha	1.19×10^{17}	1.78×10^{17}	EPHEM	Fienga (2018)
211	Isolda	1.99×10^{18}	6.84×10^{18}	DEFL	Zielenbach (2011)
211	Isolda	2.67×10^{18}	5.34×10^{18}	DEFL	Zielenbach (2011)
211	Isolda	2.41×10^{18}	5.34×10^{18}	DEFL	Zielenbach (2011)
211	Isolda	4.16×10^{18}	7.98×10^{18}	DEFL	Zielenbach (2011)
211	Isolda	7.83×10^{18}	9.39×10^{18}	EPHEM	Fienga et al. (2011)
211	Isolda	2.98×10^{18}	1.79×10^{18}	DEFL	Goffin (2014)
211	Isolda	6.36×10^{18}	6.81×10^{18}	EPHEM	Viswanathan et al. (2017)
211	Isolda	5.40×10^{18}	6.12×10^{18}	EPHEM	Fienga (2018)
238	Hypatia	4.86×10^{18}	1.25×10^{19}	DEFL	Zielenbach (2011)
238	Hypatia	5.44×10^{18}	9.81×10^{18}	DEFL	Zielenbach (2011)
238	Hypatia	6.20×10^{18}	9.72×10^{18}	DEFL	Zielenbach (2011)
238	Hypatia	8.63×10^{17}	2.18×10^{19}	DEFL	Zielenbach (2011)
238	Hypatia	2.98×10^{18}	1.79×10^{18}	DEFL	Goffin (2014)

Table D.3: continued.

#	Name	M	δM	Method	Reference
	(kg)	(kg)			
238	Hypatia	4.79×10^{18}	5.67×10^{18}	EPHEM	Fienga (2018)
266	Aline	4.23×10^{18}	6.33×10^{18}	EPHEM	Viswanathan et al. (2017)
266	Aline	1.43×10^{18}	2.08×10^{18}	EPHEM	Fienga (2018)
303	Josephina	1.31×10^{17}	1.97×10^{17}	EPHEM	Fienga (2018)
345	Tercidina	2.68×10^{18}	3.54×10^{18}	EPHEM	Fienga et al. (2011)
345	Tercidina	3.53×10^{18}	3.48×10^{18}	EPHEM	Viswanathan et al. (2017)
345	Tercidina	1.17×10^{18}	1.53×10^{18}	EPHEM	Fienga (2018)
350	Ornamenta	2.59×10^{17}	3.87×10^{17}	EPHEM	Fienga (2018)
356	Liguria	7.83×10^{18}	4.50×10^{18}	EPHEM	Fienga et al. (2011)
356	Liguria	8.30×10^{18}	3.45×10^{18}	EPHEM	Fienga et al. (2013)
356	Liguria	2.78×10^{18}	1.19×10^{18}	DEFL	Goffin (2014)
356	Liguria	3.98×10^{18}	2.11×10^{18}	EPHEM	Viswanathan et al. (2017)
356	Liguria	9.05×10^{17}	1.22×10^{18}	EPHEM	Fienga (2018)
358	Apollonia	1.60×10^{17}	2.40×10^{17}	EPHEM	Fienga (2018)
362	Havnia	1.67×10^{17}	2.51×10^{17}	EPHEM	Fienga (2018)
366	Vincentina	1.00×10^{17}	1.50×10^{17}	EPHEM	Fienga (2018)
373	Melusina	3.43×10^{17}	5.16×10^{17}	EPHEM	Fienga (2018)
377	Campania	1.52×10^{17}	2.28×10^{17}	EPHEM	Fienga (2018)
404	Arsinoe	1.25×10^{18}	3.51×10^{18}	EPHEM	Fienga et al. (2013)
404	Arsinoe	7.87×10^{17}	9.84×10^{17}	EPHEM	Fienga (2018)
405	Thia	1.38×10^{18}	4.14×10^{17}	EPHEM	Folkner et al. (2009)
405	Thia	2.74×10^{18}	1.97×10^{18}	EPHEM	Fienga et al. (2013)
405	Thia	6.38×10^{18}	1.12×10^{18}	EPHEM	Fienga et al. (2014)
405	Thia	2.19×10^{18}	2.98×10^{18}	DEFL	Goffin (2014)
405	Thia	3.13×10^{18}	1.39×10^{18}	EPHEM	Viswanathan et al. (2017)
405	Thia	2.80×10^{18}	1.28×10^{18}	EPHEM	Fienga (2018)
407	Arachne	1.26×10^{17}	1.88×10^{17}	EPHEM	Fienga (2018)
410	Chloris	6.11×10^{18}	2.76×10^{18}	EPHEM	Fienga et al. (2011)
410	Chloris	6.91×10^{18}	3.93×10^{18}	EPHEM	Fienga et al. (2013)
410	Chloris	5.33×10^{18}	2.58×10^{18}	EPHEM	Viswanathan et al. (2017)
410	Chloris	1.89×10^{18}	1.79×10^{18}	EPHEM	Fienga (2018)
442	Eichsfeldia	2.50×10^{17}	3.69×10^{17}	EPHEM	Fienga (2018)
445	Edna	4.18×10^{18}	3.57×10^{18}	DEFL	Goffin (2014)
445	Edna	1.24×10^{18}	1.83×10^{18}	EPHEM	Fienga (2018)
481	Emita	1.31×10^{18}	1.87×10^{18}	EPHEM	Fienga (2018)
488	Kreusa	2.46×10^{18}	7.38×10^{17}	EPHEM	Folkner et al. (2009)
488	Kreusa	1.60×10^{19}	1.85×10^{19}	DEFL	Zielenbach (2011)
488	Kreusa	2.29×10^{18}	1.99×10^{18}	DEFL	Zielenbach (2011)
488	Kreusa	2.19×10^{18}	2.00×10^{18}	DEFL	Zielenbach (2011)
488	Kreusa	8.25×10^{17}	4.11×10^{19}	DEFL	Zielenbach (2011)
488	Kreusa	9.77×10^{18}	8.10×10^{18}	EPHEM	Fienga et al. (2011)
488	Kreusa	1.03×10^{19}	1.08×10^{19}	EPHEM	Fienga et al. (2013)
488	Kreusa	8.58×10^{17}	1.01×10^{19}	EPHEM	Fienga et al. (2014)
488	Kreusa	7.36×10^{18}	2.98×10^{18}	DEFL	Goffin (2014)
488	Kreusa	4.65×10^{18}	5.58×10^{18}	EPHEM	Viswanathan et al. (2017)
488	Kreusa	4.63×10^{18}	5.28×10^{18}	EPHEM	Fienga (2018)
490	Veritas	9.32×10^{18}	1.31×10^{19}	DEFL	Zielenbach (2011)
490	Veritas	4.48×10^{18}	6.33×10^{18}	DEFL	Zielenbach (2011)
490	Veritas	4.59×10^{18}	6.30×10^{18}	DEFL	Zielenbach (2011)
490	Veritas	9.51×10^{18}	1.69×10^{19}	DEFL	Zielenbach (2011)
490	Veritas	2.02×10^{18}	2.96×10^{18}	EPHEM	Fienga (2018)
503	Evelyn	8.28×10^{17}	1.15×10^{18}	EPHEM	Fienga (2018)
521	Brixia	7.09×10^{17}	1.01×10^{18}	EPHEM	Viswanathan et al. (2017)
521	Brixia	3.37×10^{17}	4.98×10^{17}	EPHEM	Fienga (2018)
554	Peraga	6.59×10^{17}	1.98×10^{17}	EPHEM	Folkner et al. (2009)
554	Peraga	7.95×10^{17}	5.97×10^{17}	DEFL	Goffin (2014)

Table D.3: continued.

#	Name (kg)	\mathcal{M} (kg)	$\delta\mathcal{M}$	Method	Reference
554	Peraga	2.34×10^{17}	3.78×10^{17}	EPHEM	Fienga (2018)
602	Marianna	3.20×10^{18}	4.08×10^{18}	EPHEM	Fienga (2018)
654	Zelinda	1.35×10^{18}	4.05×10^{17}	EPHEM	Folkner et al. (2009)
654	Zelinda	6.76×10^{18}	2.98×10^{18}	DEFL	Goffin (2014)
654	Zelinda	7.41×10^{17}	7.83×10^{17}	EPHEM	Fienga (2018)
694	Ekard	1.20×10^{17}	1.78×10^{17}	EPHEM	Fienga (2018)
735	Marghanna	7.23×10^{17}	8.94×10^{17}	EPHEM	Fienga (2018)
751	Faina	3.27×10^{18}	1.75×10^{18}	EPHEM	Fienga et al. (2011)
751	Faina	4.53×10^{18}	3.30×10^{18}	EPHEM	Viswanathan et al. (2017)
751	Faina	4.13×10^{18}	3.03×10^{18}	EPHEM	Fienga (2018)
776	Berbericia	5.46×10^{18}	1.41×10^{19}	DEFL	Zielenbach (2011)
776	Berbericia	2.39×10^{16}	9.78×10^{18}	DEFL	Zielenbach (2011)
776	Berbericia	3.08×10^{17}	9.72×10^{18}	DEFL	Zielenbach (2011)
776	Berbericia	6.28×10^{18}	2.19×10^{19}	DEFL	Zielenbach (2011)
776	Berbericia	8.11×10^{18}	6.69×10^{18}	EPHEM	Fienga (2018)
788	Hohensteina	1.85×10^{17}	2.77×10^{17}	EPHEM	Fienga (2018)
791	Ani	1.47×10^{17}	2.21×10^{17}	EPHEM	Fienga (2018)
914	Palisana	1.97×10^{18}	2.16×10^{18}	EPHEM	Viswanathan et al. (2017)
914	Palisana	4.89×10^{17}	6.87×10^{17}	EPHEM	Fienga (2018)
1467	Mashona	2.04×10^{17}	3.06×10^{17}	EPHEM	Fienga (2018)